DOKUZ EYLÜL UNIVERSITY

GRADUATE SCHOOL OF NATURAL AND APPLIED SCIENCES

A NUMERICAL STUDY ON A BOREHOLE HEAT EXCHANGER WITH PHASE CHANGE MATERIAL

by

Nezir Yağız ÇAM

January, 2021

İZMİR

A NUMERICAL STUDY ON A BOREHOLE HEAT EXCHANGER WITH PHASE CHANGE MATERIAL

A Thesis submitted to
the Graduate School of Natural Sciences of Dokuz Eylül University
In Partial Fulfillment of the Requirements for the Degree of Master of Science
in Mechanical Engineering, Thermodynamics Program

by

Nezir Yağız ÇAM

January, 2021

İZMİR

M.Sc THESIS EXAMINATION RESULT FORM

We have read thesis entitled "**A NUMERICAL STUDY ON A BOREHOLE HEAT EXCHANGER WITH PHASE CHANGE MATERIAL**" completed by **NEZİR YAĞIZ ÇAM** under supervision of **ASSOC.PROF.DR. MEHMET AKİF EZAN** and **ASST. PROF. DR. LEVENT BİLİR** we certify that in our opinion it is fully adequate, in scope and in quality, as a thesis for the degree of Master of Science.

Assoc. Prof. Dr. Mehmet Akif EZAN

Supervisor

Asst. Prof. Dr. Levent BİLİR

Supervisor

Prof. Dr. Aytunç EREK

(Jury Member)

Assoc. Prof Dr. Alpaslan TURGUT

(Jury Member)

Asst. Prof. Dr. Ziya Haktan KARADENİZ

(Jury Member)

Prof. Dr. Özgür ÖZÇELİK
Director
Graduate School of Natural and Applied Sciences

ACKNOWLEDGEMENTS

Firstly, I would like to thank my co-advisors Assoc. Prof. Dr. Mehmet Akif EZAN and Asst. Prof. Dr. Levent BILIR for their guidance supports and for allowing me to study the topic I passionately love.

I also would like to thank Res. Asst. Ersin ALPTEKIN for his support and contributions in the period of research.

I wish to express my thanks to my friends at the Department of Mechanical Engineering for their support and help.

Essentially, I thank my parents, Uğur and Melek ÇAM, for their patience, endless support, and advice.

Nezir Yağız ÇAM

A NUMERICAL STUDY ON A BOREHOLE HEAT EXCHANGER WITH PHASE CHANGE MATERIAL

ABSTRACT

This study aims to develop a dynamic numerical model in MATLAB to evaluate the parameters that affect the solar-assisted borehole thermal energy storage unit's performance filled with different materials under variable weather conditions. Moreover, another purpose of the study is to investigate the effect of a thermal energy storage system when it is integrated with a heat pump, which is used for heating purposes in Izmir City, Turkey.

In the first stage of the thesis, an in-house model is developed to simulate the solar aided borehole heat storage unit that is run with different backfill materials such as clay, soil, and PCM integrated soil domain. The effects of PCM implementation into the backfill domain decreases the heat diffusion within the backfill domain and provides keeping thermal energy around the pipe. Furthermore, weather conditions such as solar irradiance, ambient air temperature, and wind velocity are the key factors of the solar-assisted borehole thermal energy storage systems. The dynamic model that is developed in the first part of the thesis is extended to integrate a latent heat thermal storage system with a heat pump unit. In this integrated model, the cyclic behavior of the latent heat energy storage unit is simulated under different heat demand profiles. Integrating the latent thermal energy storage system into the heat pump results in an increase in the heat pump performance coefficient between 1.3 and 1.8 times.

Keywords: Borehole heat exchanger, phase change material, thermal energy storage, integrated systems

FAZ DEĞİŞİM MALZEMELİ KUYU İÇİ ISI DEĞİŞTİRİCİSİ ÜZERİNE SAYISAL ÇALIŞMA

ÖZ

Bu çalışma, değişken hava koşullarında farklı malzemelerle doldurulmuş güneş destekli sondaj termal enerji depolama ünitesinin performansını etkileyen parametreleri araştırmak için MATLAB'da dinamik bir sayısal model geliştirmeyi amaçlamaktadır. Ayrıca çalışmanın bir diğer amacı, İzmir ilinde ısıtma amaçlı kullanılan bir ısı pompası ile entegre edildiğinde bir termal enerji depolama sisteminin etkisini değerlendirmektir.

Tezin ilk aşamasında, kil, toprak ve FDM entegre toprak alanı gibi farklı dolgu malzemeleri ile çalıştırılan güneş destekli kuyu içi ısı depolama ünitesini simüle etmek için bir model geliştirilmiştir. FDM uygulamasının dolgu alanına etkileri, dolgu alanındaki ısı yayılımını azaltır ve termal enerjinin boru çevresinde tutulmasını sağlar. Ayrıca, güneş ışınımı, ortam sıcaklığı ve rüzgar hızı gibi hava koşulları, güneş destekli kuyu içi termal enerji depolama sistemlerinin temel faktörleridir. Tezin ilk bölümünde geliştirilen dinamik model, bir gizli ısı termal depolama sistemini bir ısı pompası ünitesi ile entegre edecek şekilde genişletilmiştir. Bu genişletilmiş modelde, gizli ısı enerjisi depolama ünitesinin döngüsel davranışı, farklı ısı talep profilleri altında simüle edilir. Gizli termal enerji depolama sistemini ısı pompasına entegre etmek, ısı pompası performans katsayısında 1,3 ile 1,8 kat arasında bir artışa neden olur.

Anahtar kelimeler: Kuyu içi ısı değiştiricisi, faz değişim malzemesi, ısıl enerji depolama, entegre sistemler

CONTENTS

Page

LIST OF FIGURES

Page

LIST OF TABLES

Page

CHAPTER ONE

INTRODUCTION

The fundamental aspects of thermal energy storage (TES) and borehole thermal energy storage (BTES) systems are given in this chapter. Solar energy-aided TES systems integrated with BTES systems are then briefly introduced, and recent works in this field are summarized.

1.1 Introduction to the TES

Due to the global climatic problems that have arisen in recent years, humanity is urged to meet energy requirements from renewable energy sources rather than fossil resources. However, the nature of renewables, such as solar and wind, is intermittent. This means that there is a difference between the periods when renewable energy sources are available and when the demand is present. Thermal energy storage (TES) systems eliminate this difference by storing renewable energy to use it when it is needed. The main processes within a TES unit consist of 3 stages as

1. Charging
2. Storage (Idle)
3. Discharging

The charging process initiates when renewable energy is highly available and terminates when the source is diminished. The charging process is simply increasing the internal energy of the storage domain in heating applications (Dinçer & Ezan, 2018). Until the discharging stage, the stored thermal energy is kept within the TES unit to supply through the demand-size. The discharging process begins when the demand arises, and the stored thermal energy is discharged from the TES unit by decreasing the internal energy of the storage domain (Dinçer & Ezan, 2018). The methods that are widely used to store heat within the TES unit are listed as:

1. Sensible heat
2. Latent heat
3. Thermochemical heat

A basic renewable energy sourced energy storage system is illustrated in Figure 1.1. In such an integrated system, the solar acting on the solar collector is transferred through the carrier fluid that is passing through the heat exchanger underneath the absorber plate. The hot working fluid is then directed through the TES tank to increase the internal energy of the storage domain, either solid or liquid media, for further usage. The stored energy within the TES unit could be directly used in residential applications such as supplying hot water supply or space heating. TES tanks could be used as a component of a more complicated system to maintain a continuous heat supply for integrated systems.

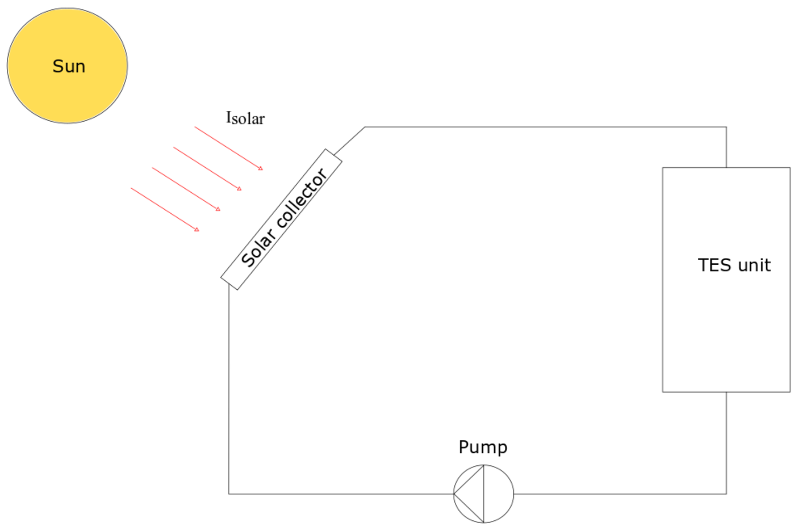

Figure 1.1 Schematic of renewable energy sourced energy storage unit

According to International Energy Agency (IEA) Key World Energy Statistics Report 2020 (IEA, 2020), 7.5% of coal, 5.4% of oil, and 29.9% of natural gas are consumed in residential applications for heating purposes. Considering the worldwide concern on environmental problems, it is important to use renewable energy-assisted thermal energy storage systems in residents by integrating with heating and cooling systems. The charging and discharging period of solar energy assisted TES unit integrated with a heat pump is schematically presented in Figure 1.2 for charging and discharging processes.

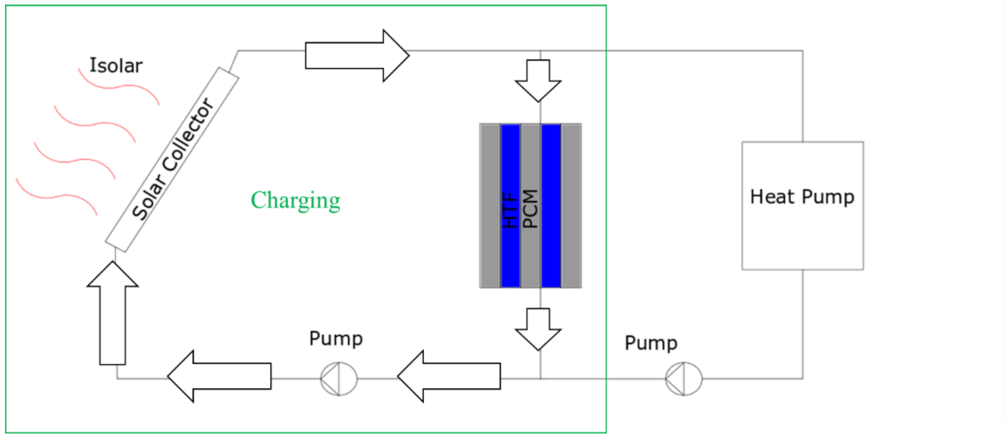

(a) Charging

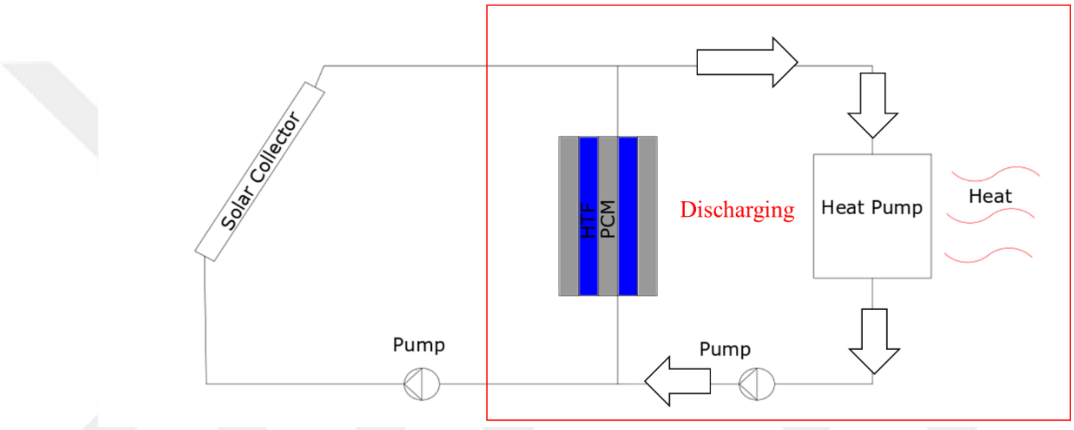

(b) Discharging

Figure 1.2 Charging and discharging period of solar energy assisted TES unit

In the discharging period of the TES, stored thermal energy is used to provide the heat demand of the heat pump, and the heat pump meets the heating requirement of the building. So, thermal energy storage systems ensure that solar energy or waste heat is not used outside of energy needs. Some techniques of TES for building applications are shown in Figure 1.3.

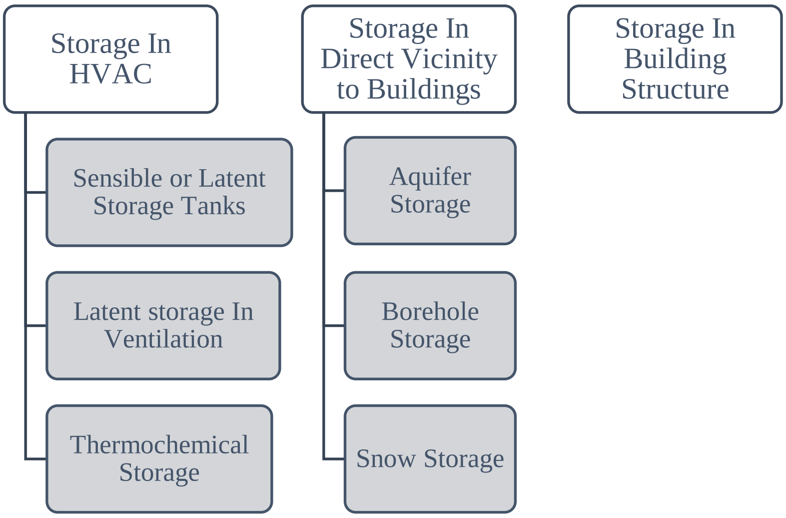

Figure 1.3 Techniques of TES for buildings Dinçer & Ezan (2018)

Although many different TES systems are in use, latent heat energy storage systems are widely used due to isothermal behavior and the high energy storage capacity of phase change materials.

1.2 Introduction of the BTES

Borehole heat exchangers (BHEs) are commonly used with ground source heat pumps. BHEs are also used for seasonal heat storage, and such systems are known as borehole thermal energy storage (BTES) systems. BTES systems consist of pipe, backfill material, and soil medium.

The design of BHE should be unique for the application to supply the energy need or store energy requirements. Geometrical parameters, types of pipe, and backfill material within the BHE are essential properties that affect the thermal performance of the BHEs. A schematic of a U-tube BHE is given in Figure 1.4.

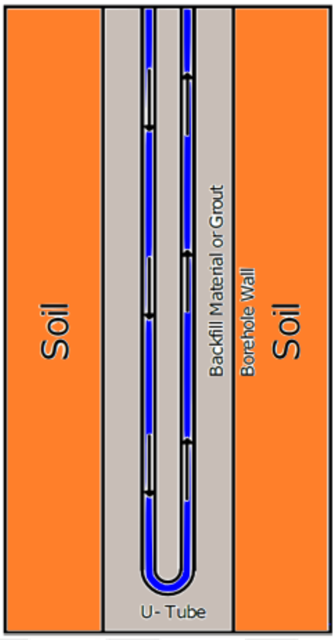

Figure 1.4 Schematic of U-Tube BHE

1.3 Literature survey

1.3.1 Literature survey on BHE and BTES

BHE are generally used with ground source heat pumps to transfer heat from the ground to the refrigerant. BHE consists of pipe, backfill material, and soil around the borehole. In recent years, BHE is also used as a thermal energy storage system due to the temperature distribution within the ground. Soil temperature becomes constant beyond a certain depth. However, experimental investigations are not easy for deep vertical BHEs because of their capital cost. Researchers mostly develop mathematical models to analyze the thermal performance of BHEs. One of the most comprehensive studies for BHE simulations was thermal resistance modeling by Eskilson & Claesson (1988). In Eskilson & Claesson's work, the thermal resistances among the components in BHE are defined as a delta circuit, and this model has provided an important opportunity to simulate BHE. Hellstörm (1991) developed a numerical model using the thermal resistance network approach to simulate different types of BHE. Bauer, Heidemann & Diersch (2011) examined the thermal performance of a BHE using soil as a filling material by defining a constant inlet temperature of heat transfer fluid

(HTF). They concluded that the diameter of the thermal influence decreases as the depth increases. Rees and He (2013) developed a numerical model with ANSYS software for the vertical borehole heat exchanger and validated the model experimentally. They varied the velocity of heat transfer fluid to investigate its influence on the thermal performance of the heat exchanger. Cui, Yang & Fang (2008) developed a model to simulate BHE under short-term working conditions using the finite element method for a vertical-type heat exchanger. They compared the predictions against the results of Eskilson & Claesson (1988). In the literature, besides mathematical models related to BHE, some studies have been made for different BHE usage purposes.

The BHE has become an essential part of underground thermal energy storage systems and is used to provide heat exchange between the heat source and refrigerant in heat pump systems. Li, Tong, Duanmu & Lui (2016) investigated the effects of the filling material radius and the filling material. They compared the thermal effect radius of the concrete and the usage of the shape stabilized PCM and the organic PCM. They concluded that the thermal energy is stored around the pipe wall when organic PCM was used as a backfill material. Bottarelli et al. (2015) modeled a shallow horizontal type borehole heat exchanger. They made a comparison between other backfilling materials in a shallow horizontal borehole heat exchanger. As a result of the study, when the phase change material is integrated, the thermal energy influence radius is considerably reduced, which means that the thermal energy is stored around the pipe wall of shallow horizontal BHE. Biglarian, Abbaspour & Saidi (2017) implemented a thermal resistance network approach into the numerical model to investigate the heat transfer in the BHE. In their work, the soil is used as backfill material, and the initial temperature of the soil is greater than the initial temperature of carrier fluid. The outlet temperature of BHE was observed.

1.3.2 Literature survey on LHTES

Trp (2005) formed a mathematical model to simulate the charging and discharging process of a shell-tube latent heat thermal energy storage unit in FORTRAN and validated the simulation results with experimental work. It is suggested that if the water is used as a working fluid in the TES unit, the heat transfer in the TES can be numerically solved as a single domain. Seddegh, Wang & Henderson (2015) developed a numerical simulation to observe vertical LHTES units' thermal behavior during charging and discharging processes under constant heat transfer fluid inlet temperature. Seddegh, Wang & Henderson (2016) investigated thermal characteristics of shell-and-tube LHTES systems during the charging and discharging processes. Effects of different HTF inlet temperature and mass flow rates on latent heat thermal energy storage performance in horizontal and vertical heat storage units are evaluated. They concluded that HTF inlet temperature has a more significant effect on the thermal performance of the LHTES than HTF mass flow rates. Mehta, Solanki, Rathod & Banerjee (2019) examined the influence of the orientation on shell-tube latent heat thermal energy storage units with annulus filled with phase change material. It is concluded that orientation played an critical role in the charging process. Tao & He (2011) developed a mathematical model to simulate PCM integrated shell-tube LHTES unit under non-steady working fluid inlet temperature and mass flow rate. They determined that increasing working fluid inlet temperature caused a decrease in melting time. Kant, Shukla, Sharma & Biwole (2018) observed charging and discharging thermal behavior of the PCM under constant and variable heat flux. Results showed that variable heating and cooling provides faster melting and solidification. Wang et al.(2013) studied the transient behavior of a TES model with PCM filling shell-tube heat exchanger under charging and discharging processes. Effects of different heat transfer fluid inlet temperature and mass flow rate on phase change material integrated thermal energy storage was observed. It was concluded that the unit reached the steady-state more quickly in the discharging process. Yu, Li, Lu, Huang & Roskilly (2019) investigated the effects of different PCMs, and different carrier fluid inlet temperature on the thermal energy storage unit integrated ORC. They concluded that fluctuation of the heat source is reduced by using PCM integrated TES units. Trp, Lenic & Frankovic (2006) investigated the influence of working fluid inlet boundaries and LHTES unit geometric parameters on the TES. It is concluded that determining operation intervals and geometric parameters are essential and should satisfy the required heat transfer and stored energy need. These parameters must be selected wisely. Başal & Ünal (2013) formed a mathematical model to investigate the performance of a triple concentric tube LHTES system in FORTRAN. Effects of different mass flow rates and inlet temperatures of working fluids on latent heat thermal energy storage units were investigated. Huang et al. (2020) studied the PCM-filled TES unit's thermal behavior integrated with a solar water heating system working under real-time boundary conditions in TRNSYS. Different system configurations were studied, and also the effects of different PCM parameters were investigated. Increasing the thermal conductivity of the PCM had improved the system efficiency significantly. Integrating the latent heat TES unit to the solar aided water heating system enhanced the heat storage capacity, and it caused less solar collector area needed to supply the demand. Elbahjoui, El Qarnia & Naimi (2018) studied the thermal performance of a solar domestic hot water system using a storage tank with various forms of tubes in Marrakesh. Triple concentric tubes have stored much higher thermal solar energy by sensible and latent heat.

1.4 Thesis motivation

The thesis aims to develop transient numerical models to investigate the thermal behaviors of two different solar-assisted systems as (i) BHE with PCM and (ii) heat pump unit with LHTES unit. In the literature, many studies have been conducted to evaluate the thermal behavior of the BHE experimentally and numerically. Also, several numerical models have been undertaken recently to simulate BHE with PCM. These studies focus on stand-alone BHE units with PCM under constant boundary conditions. However, BHEs, either w/ PCM or w/o PCM, are mostly used integrated with solar collectors or/and heating and cooling systems. The thesis focuses on this gap in the literature.

In the first part of the thesis, an in-house numerical code is developed to investigate the cyclic behavior of a solar-aided BHE to investigate the effects of integrating PCM into the BHE unit backfill materials that are used in real applications. Further, the effects of real weather conditions on the solar-assisted BHE unit are investigated in the first part of the thesis. In the second part of the thesis, a transient model to investigate the solar aided LHTES unit integrated with a heat pump to supply the heat demand of a house in Izmir under real weather conditions is developed in MATLAB. The effects of demand profile, latent heat, and melting temperature of PCMs on the thermal behavior of solar aided LHTES units are investigated. Besides, the effect of integrating a solar-assisted LHTES unit into a heat pump is evaluated within an energetic view. The flowchart of the current thesis is presented in Figure 1.5.

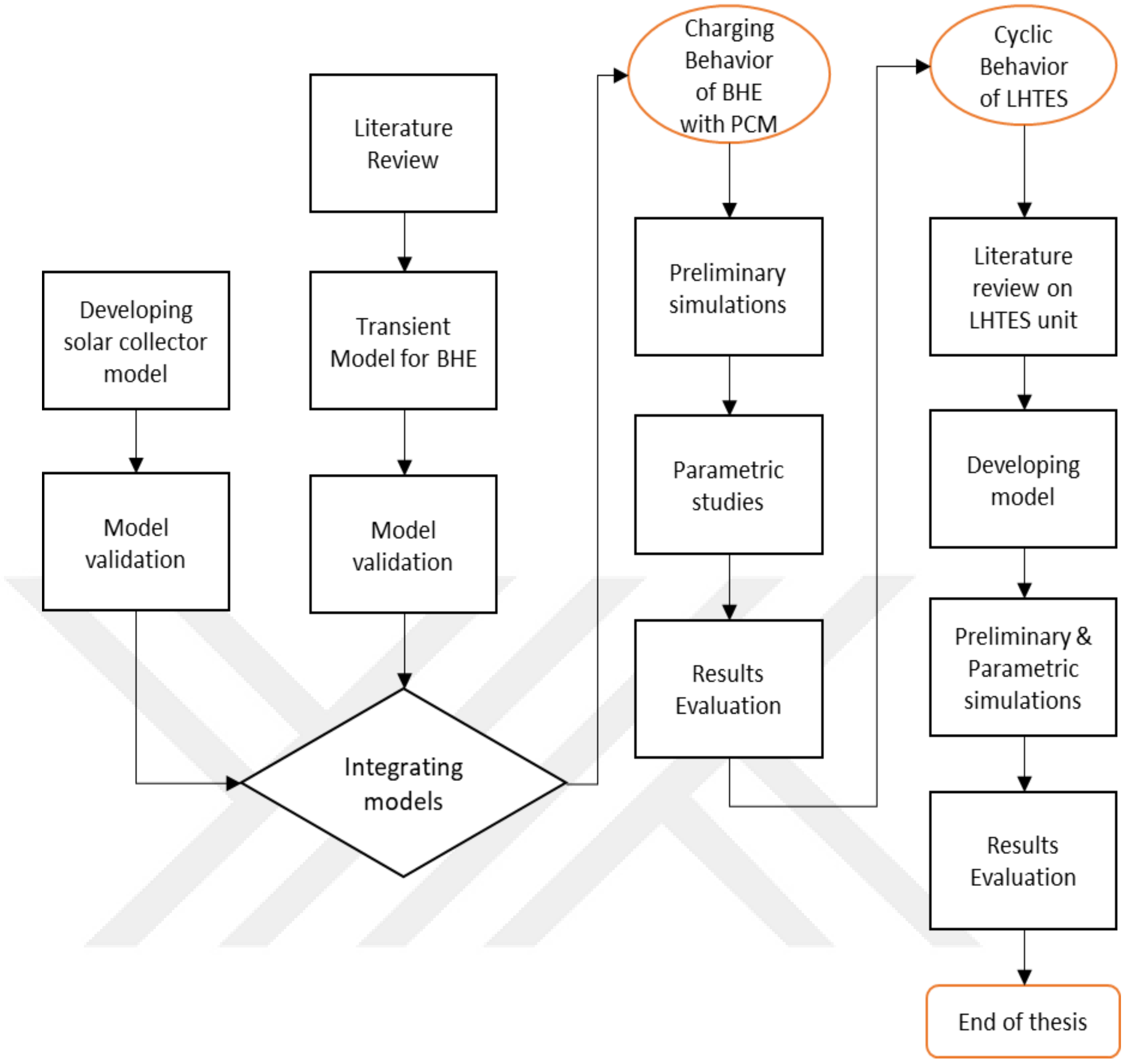

Figure 1.5 Flow chart of thesis

CHAPTER TWO

CHARGING BEHAVIOR OF BOREHOLE HEAT EXCHANGER WITH PHASE CHANGE MATERIAL

In this chapter, a numerical model is developed to investigate the influence of PCM usage in a solar-assisted BHE unit on the charging behavior. This chapter defines the system with boundary conditions, represents the solution method, and discusses the simulation results.

2.1 Problem Definition

In this study, a solar-assisted BHE unit filled with soil, clay, and soil with PCM domain on the charging process is simulated for a day on heating months in Izmir, i.e., November, December, January, February, and March. Investigations are made to determine the influence of backfill materials and integrating PCM into the BHE unit on charging behavior and thermal influence radius with the transient model developed in MATLAB. A lumped solar collector model is developed and integrated into the primary model to consider the variable weather conditions. The HTF temperature increases within the pipes of the solar collector, and then the HTF heats the backfill material while flowing through the BHE unit. The schematic of the BHE unit is shown in Figure 2.1. The length of the BHE is defined as $L = 0.5\ m$.

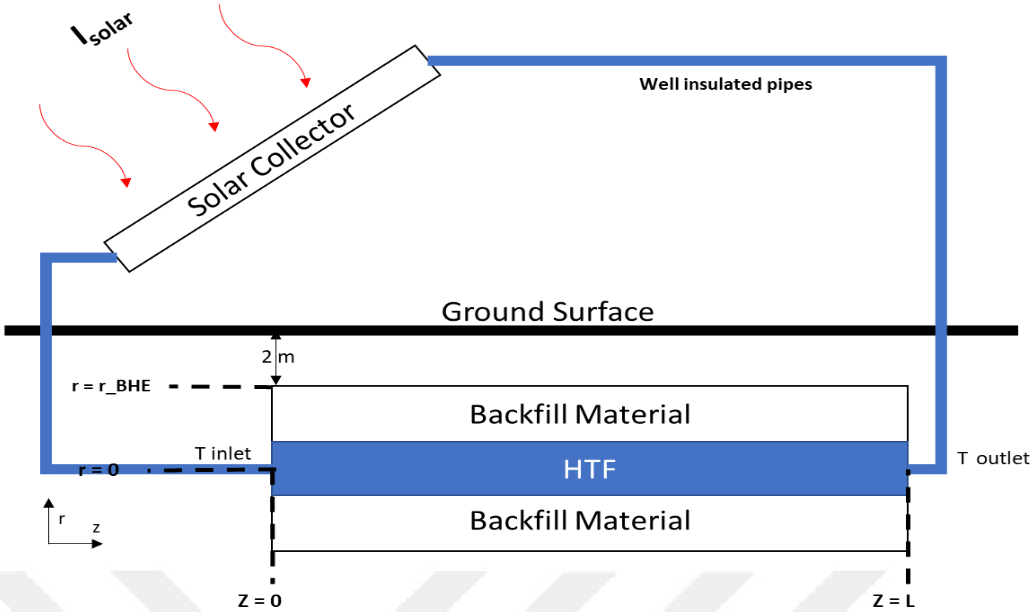

Figure 2.1 Schematic of solar-assisted BHE unit

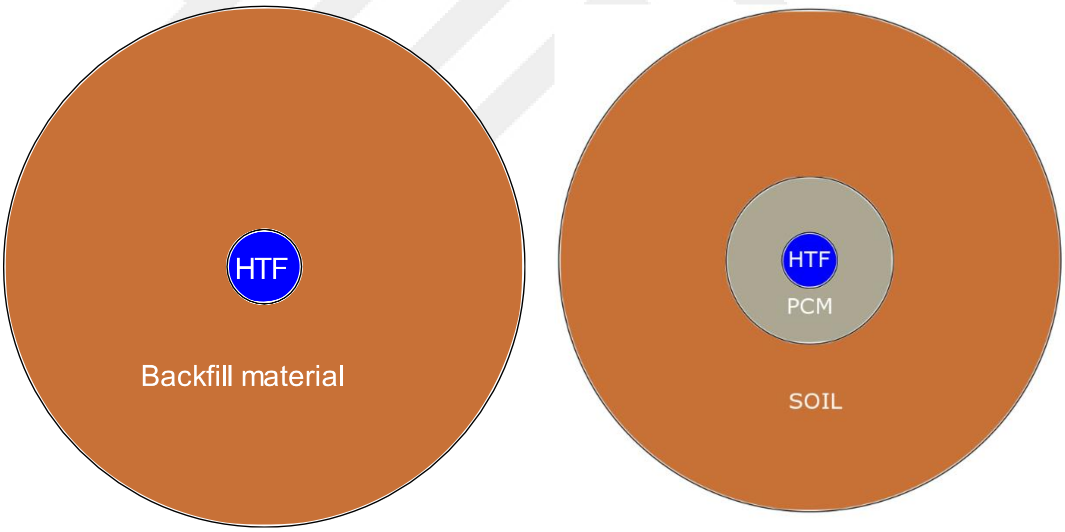

(a) w/o PCM (b) w/ PCM

Figure 2.2 Top view of BHE unit (a) w/o PCM (b) w/PCM

In Figure 2.2, the top view of BHE units w/o PCM and w/ PCM is illustrated. Clay and soil are used as backfill material for w/out PCM case. The thermophysical properties of the operating fluid and backfill materials, i.e., clay, soil, and PCM, are given in Table 2.1. Soil and clay as a backfill material are assumed to be dry, and the thermophysical properties of soil are taken from Bergman, Incropera, DeWitt & Lavine (2011). The melting temperature of the PCM is selected as $T_m = 31$°C.

Table 2.1 Thermophysical properties of materials

		Thermal conductivity (W/mK)	Specific Heat (J/kg)	Density (m^3/kg)	References
Water		0.576	4180	1000	Bergman et al. (2011)
PCM	Solid	0.18	1800	789	Rubitherm (2018)
	Liquid	0.19	2400	750	Rubitherm (2018)
Soil		0.52	1840	2050	Bergman et al. (2011)
Clay		1.675	920	1495	Bergman et al. (2011)

The design parameters of the BHE unit and solar collector are given in Table 2.2. D_{pipe} denotes the diameter of pipe within BHE. D_{pcm} is the diameter of the PCM layer, and D_{BHE} designate the diameter of the BHE.

Table 2.2 Design parameters of the model

Parameter	Value	Units	Parameter	Value	Units
D_{pipe}	0.025	m	ε_{plate}	0.98	-
D_{pcm}	0.05	m	ε_{cover}	0.88	-
D_{BHE}	1	m	α	0.97	-
τ	0.9	-	β	30.3	º
W_{col}	1	m	k_{plate}	0.03	W/mK
H_{col}	2.5	m	$D_{pipe,col}$	0.02	m
$w_{s,col}$	0.115	m	U_{inlet}	0.01	m/s

The charging process of the BHE unit starts at 8 am. The working fluid flows through the solar collector, gains energy from the solar irradiance, and then transfers thermal energy to the backfill material within the BHE unit until 3 pm. The charging hours are decided according to the results of preliminary analyses. The irradiance before 8 am is not adequate for the operation and, the working fluid temperature reduces within the solar collector because of the ambient temperature beyond 3 pm. So, the duration of the charging process is decided in such a way to minimize such losses. In the process of charging, the HTF circulates through an installed pipe circuit and gains heat by passing through the solar collector and transfers the heat to the backfill material. In the w/o PCM case, in which clay and soil are used as backfill material, the thermal energy storage technique is sensible heat storage. When the PCM is integrated within the BHE, energy is stored via both sensible and latent heat.

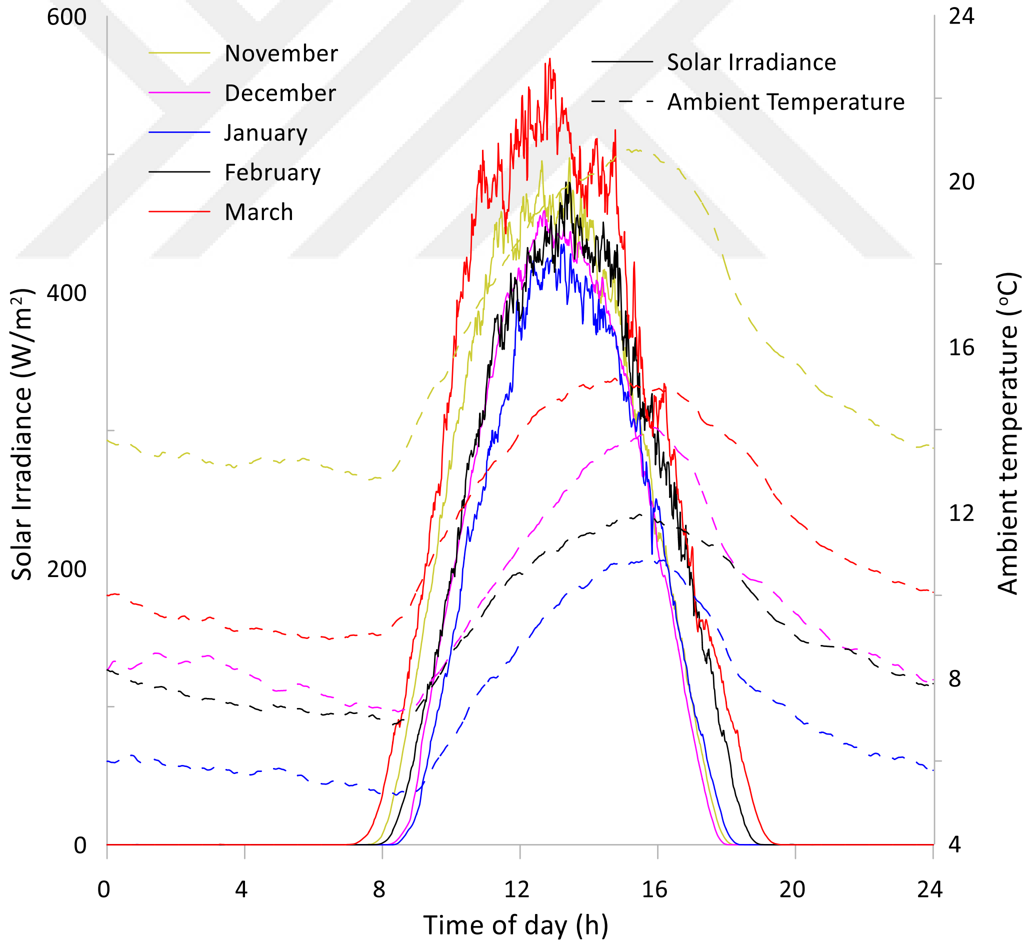

Figure 2.3 Weather data of Izmir

Real weather data used in the developed numerical model for November, December, January, February, and March are given in Figure 2.3.

2.2 Solution Methods

In this subsection, the methods that are used in the in-house code to investigate the charging behavior of the solar-assisted BHE unit are briefly explained.

2.2.1 Governing equations

In the current thesis, the following assumptions are made to develop a numerical model for simulating the BHE unit.

(1) The inlet velocity of the working fluid is constant.
(2) The soil temperature at the 2 m soil depth is 10 ℃.
(3) The BTES unit and circulating pipes are well insulated.
(4) The initial temperature within the BTES unit is equal to soil temperature.
(5) The fluid is fully developed.
(6) The free convection in the PCM domain is neglected.

The governing equation of the working fluid domain is reduced into the following form

for PCM domain:

$$\frac{\partial CT}{\partial t} = \frac{\partial}{\partial z}\left(k\frac{\partial T}{\partial z}\right) + \frac{1}{r}\frac{\partial}{\partial r}\left(kr\frac{\partial T}{\partial r}\right) - \frac{\partial S}{\partial t} \tag{2.1}$$

for working fluid domain:

$$\rho c\frac{\partial T}{\partial t} + \rho c u\frac{\partial T}{\partial z} = \frac{\partial}{\partial z}\left(k\frac{\partial T}{\partial z}\right) + \frac{1}{r}\frac{\partial}{\partial r}\left(kr\frac{\partial T}{\partial r}\right) \tag{2.2}$$

The dimensionless numbers for the working fluid domain are calculated by using the following equations

for Reynolds number:

$$Re = \rho \frac{U_{inlet} D_{pipe}}{\mu} \tag{2.3}$$

where U_{inlet} is inlet velocity of the working fluid, D_{pipe} is the diameter of the pipe, k_{HTF} is the thermal conductivity of the operating fluid and μ_{HTF} is the viscosity of the operating fluid.

for Prandtl number:

$$Pr = \frac{\mu_{HTF} c_{HTF}}{k_{HTF}} \tag{2.4}$$

The Reynolds number is calculated as $Re = 511.2474$ so the flow is laminar and since the flow is assumed fully developed, the Nusselt number is found as follows.

$$Nu = 3.66 \tag{2.5}$$

The followed equation is used for the convective heat transfer coefficient:

$$h_{conv} = \frac{Nu k_{HTF}}{D_{pipe}} \tag{2.6}$$

The heat diffusion in the PCM domain is modeled by using the fixed grid numerical model of Cao & Faghri (1990).

$$C(T) = \begin{cases} (\rho c)_s & T < T_m - \delta T_m \\ (\rho c)_m + \rho_l \dfrac{h_{sf}}{2\delta T_m} & T_m - \delta T_m \le T \le T_m + \delta T_m \\ (\rho c)_l & T > T_m - \delta T_m \end{cases} \tag{2.7}$$

$$S(T) = \begin{cases} (\rho c)_s (\delta T_m - T_m) & T < T_m - \delta T_m \\ (\rho c)_l (\delta T_m - T_m) + \rho_l \dfrac{h_{sf}}{2\delta T_m} - \rho_l \dfrac{h_{sf}}{2\delta T_m} T_m & T_m - \delta T_m \le T \le T_m + \delta T_m \\ (\rho c)_l (\delta T_m - T_m) - \rho_l h_{sf} & T > T_m - \delta T_m \end{cases} \tag{2.8}$$

A thermal resistance network is used to implement the soil domain into the PCM domain. After the location shell of PCM, additional grids are defined within the soil domain and the heat transfer with conduction is modeled by determining the thermal resistance of materials.

Thermal resistance between PCM domain and soil domain can be defined as:

$$R_{PCM-S} = \frac{\ln\left(\frac{D_i}{D_{PCM}}\right)}{2\pi k_{soil} dz} \tag{2.9}$$

where D_i represents the selected point in the soil domain, dz represents the defined grid step in the *z*-direction.

The resistance between the selected grid in the soil domain and shell of the BHE can be written as:

$$R_{S-BHE} = \frac{\ln\left(\frac{D_i}{D_{BHE}}\right)}{2\pi k_{soil} dz} \tag{2.10}$$

where D_{BHE} represents the diameter of BHE.

2.2.2 Lumped model for solar collector

Lumped model for solar collector is formed based on mathematical approach by Duffie & Beckman (2013). It is assumed that heat losses from sidewise surfaces no exists. Following equation represents the energy equation for the collector.

$$\frac{d}{dt}(\dot{m}cT)_{HTF} = \dot{Q}_u + \left[\dot{m}c\left(T_{col,in} - T_{col,out}\right)\right]_{HTF} \tag{2.11}$$

where $T_{col,in}$ and $T_{col,out}$ signify the inlet and outlet temperature of the heat transfer fluid within the solar collector, respectively. $\dot{Q}_u$ signifies the useful heat transfer to the carrier fluid. $\dot{Q}_u$ can be calculated as

$$\dot{Q}_u = A_{col} F_R [(I_{solar} \tau\alpha) - U_L \left(T_{col,in} - T_{amb}\right) \tag{2.12}$$

Alptekin & Ezan (2020), represents the detailed solution algorithm of the solar collector lumped model.

2.2.3 Solution procedure

In the numerical method, variable weather data of Izmir City is imported into the code, and the flat plate solar collector sub-function solves the related equations, i.e., Equations. 2.11 and 2.12, to compute the temperature of the HTF at the outlet of the solar collector. The outlet temperature of the solar collector is then defined as the inlet temperature of the solar aided BHE unit. The control volume method is applied for the HTF and the backfill domains to transform the governing equations for each domain, i.e., Equations. 2.1 and 2.2, into algebraic form. Moreover, thermal resistances between materials are determined, i.e., Equations 2.9 and 2.10. The final set of algebraic equations is then iteratively solved with SIS (Strongly Implicit Solver) (Lee, 1990) algorithm with 10^{-8} tolerance. The convergence criteria in the model assumed as 10^{-7} after several attempts. Also, grid size and time step determined for BHE w/PCM model after many preliminary analyses as 100×150 and $1\ s$ respectively. For the BHE w/o PCM model, the grid size is determined as 100×50 after several preliminary analyses. The iterative solver for the integrated system, which involves the solar collector and the BHE unit, is coded in MATLAB software.

2.3 Validations of developed models

The mathematical model formed to simulate the charging and discharging process of the TES unit is validated by reproducing Gong and Mujumdar (1997). Geometric parameters and thermophysical properties of the fluids and PCM are defined according to Gong and Mujumdar (1997). In Figure 2.4, the results of the current model and the results of the reference are compared.

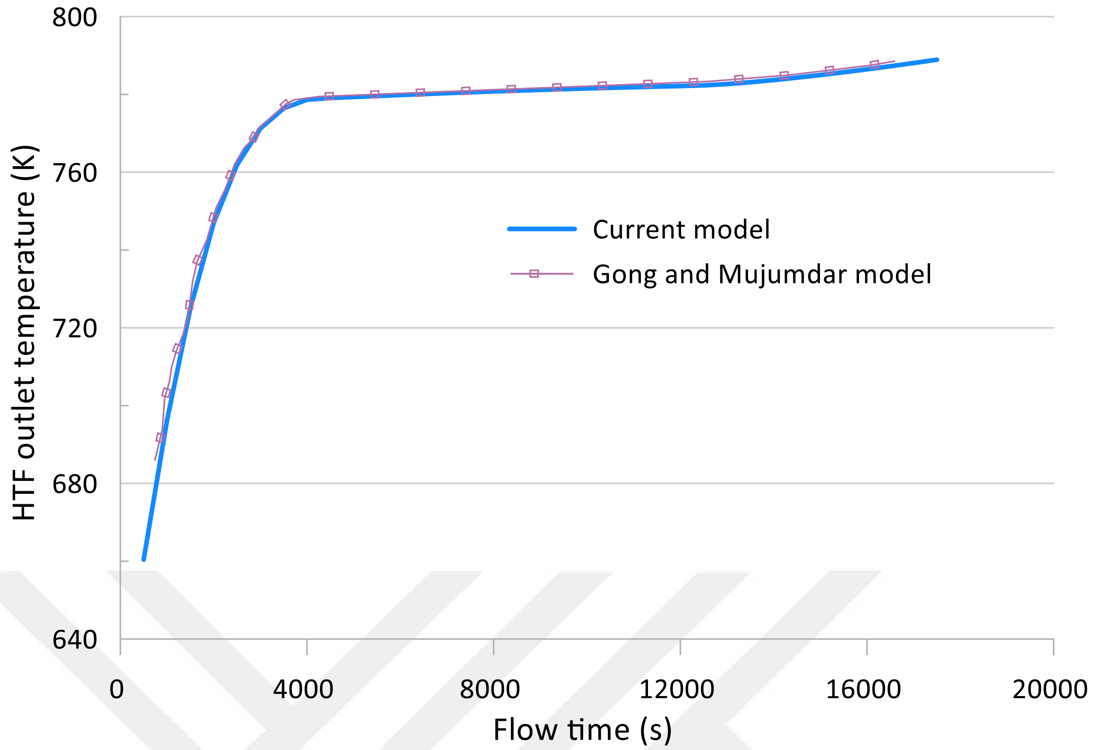

Figure 2.4 Numerical model validation

In this current thesis, a solar collector model is created to simulate heat transfer within solar collectors to heat transfer fluid. The results in Duffie & Beckman (2013) are used as a reference to validate the model's outputs. Top loss coefficient variation against the average plate temperature is investigated and compared with Duffie & Beckman (2013), as illustrated in Figure 2.5.

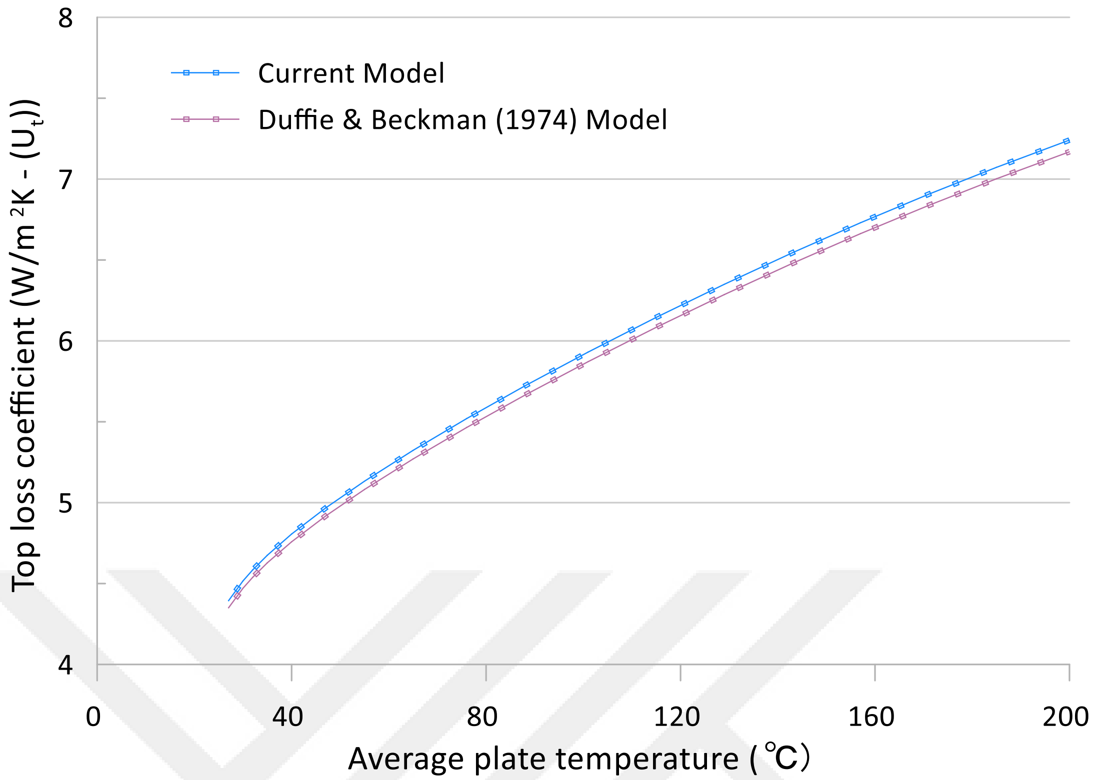

Figure 2.5 Solar collector model validation

2.4 Results & Discussion

The effect of the BTES length on the charging performance of the solar-assisted BTES with PCM and the effects of the different backfill materials on the thermal influence radius is represented in this section. Further, the results of the simulations for five different heating months are also discussed.

2.4.1 Charging period of solar-assisted BTES unit with different backfill materials

The charging behavior of the BTES unit is affected by the thermophysical properties of backfill materials used in the BTES unit. In this study, the effects of three different backfill domains on the charging behavior of the BTES unit are studied for five different heating months. Firstly, the soil is used as a backfill material within the solar-assisted BTES unit. The HTF inlet temperature into the BTES unit and mean soil temperature within the BTES unit depending on time are given in Figure 2.6.

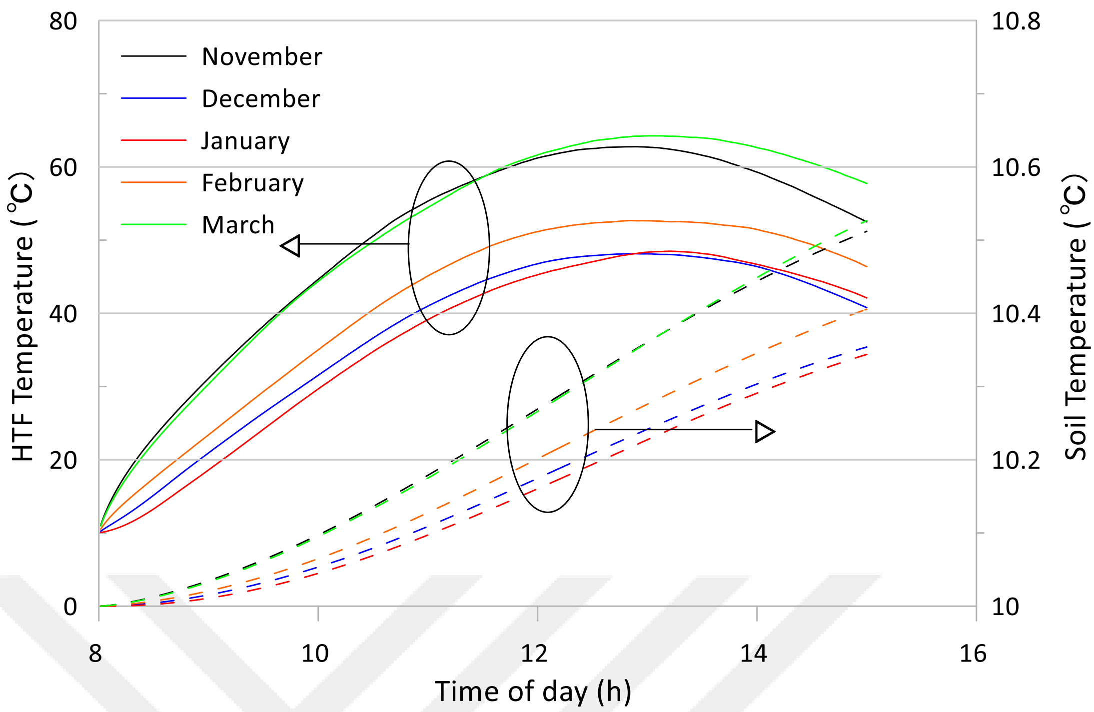

Figure 2.6 HTF inlet temperature and soil temperature change in time

As shown in Figure 2.6, the inlet temperature of the HTF increases until midday, then HTF temperature decreases in each of the selected months. The inlet temperature of the HTF increases up to 65°C in March, 63°C in November, 55°C in February, 50°C in January and December. It can be said that the ambient temperature and solar irradiance have a great impact on the HTF inlet temperature. The mean soil temperature at the end of the charging process goes up to 10.55°C, 10.35°C, 10.34°C, 10.4°C, and 10.56°C in November, December, January, February, and March, respectively.

Clay is another material used as backfill material in the BTES unit. The variations in the inlet temperature of the HTF and the mean temperature of the clay are shown in Figure 2.7. The HTF inlet temperature and clay mean temperature increases with time. The HTF inlet temperature reaches approximately 65°C at midday. The mean temperature of clay goes up to 13.5°C at the end of the charging process in March and November. However, the inlet temperature of the HTF and clay mean temperature is lower in other heating months when compared with March and November. Also, the mean temperature of the clay is higher compared to the soil's mean temperature. At the end of the charging process in March, the mean clay temperature is 13.5 °C, and the mean temperature of the soil is 10.5 °C.

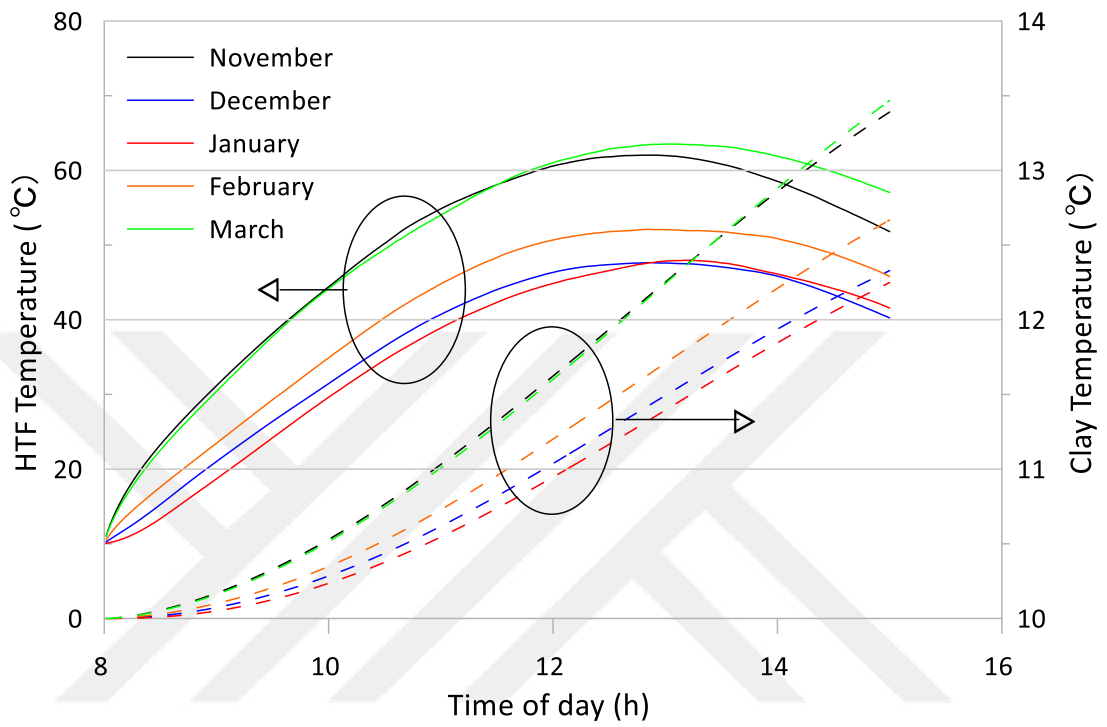

Figure 2.7 Change of HTF inlet and clay temperature in time

Dynamic simulation of the charging process of a PCM integrated BTES unit is one of the motivations of this thesis. In Figure 2.8, the variations in the inlet temperature of the HTF, the mean temperature of the PCM, the mean temperature of the soil domain, and the liquid fraction of the PCM in five different heating months are shown.

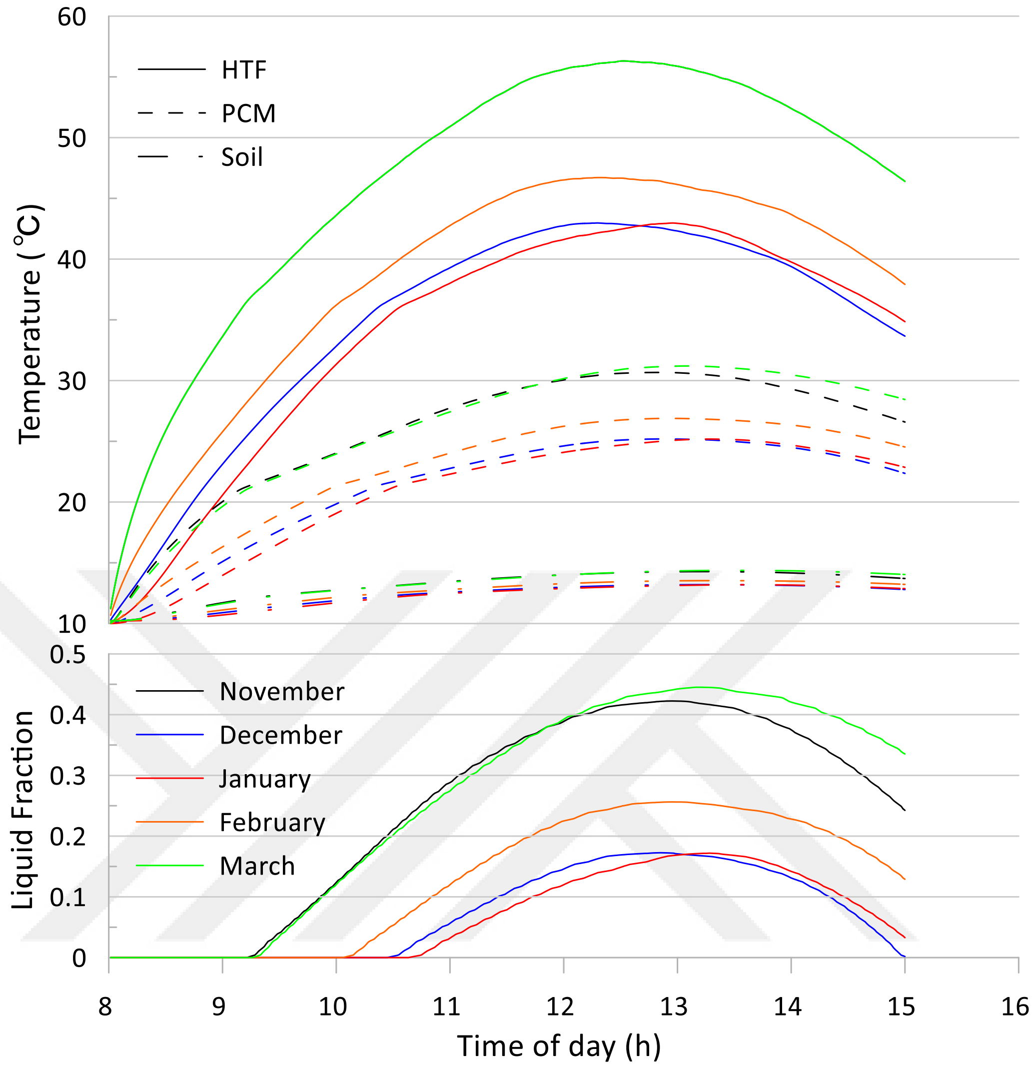

Figure 2.8 Domain temperature and liquid fraction of PCM in BHE unit

The HTF inlet temperature, the mean temperature of PCM, and soil mean temperature increase until midday. Although the HTF inlet temperature in November and March are close to each other, the mean PCM temperature in March and November differs after midday. The liquid fraction of PCM has a similar pattern with the mean temperature of PCM. In March and November, the mean PCM temperature reaches the melting temperature of the PCM ($T_m = 31$°C) at midday, however, the PCM is not completely melted in these months. The peak value of the liquid fraction reaches 0.45 in March.

The solar irradiance and ambient temperature significantly impact the HTF inlet temperature in the solar-assisted BTES unit. Also, backfill material has an influence on the performance of the system.

2.4.2 Effects of backfill material on thermal influence radius and solar collector

Thermal influence radius is defined by monitoring the temperature distributions along the radial direction of the BTES. In Figure 2.9, the temperature distributions within the backfill domain at the mid-height of the BTES unit, i.e., $z = 0.250$ m, along the radial direction are given. The temperature variations are given for the clay, soil, and PCM domains at $t = 9000$ s and $t = 18000$ s. The pipe radius and the radius of the PCM domain for the case that PCM is integrated within the BTES unit are given in the figure.

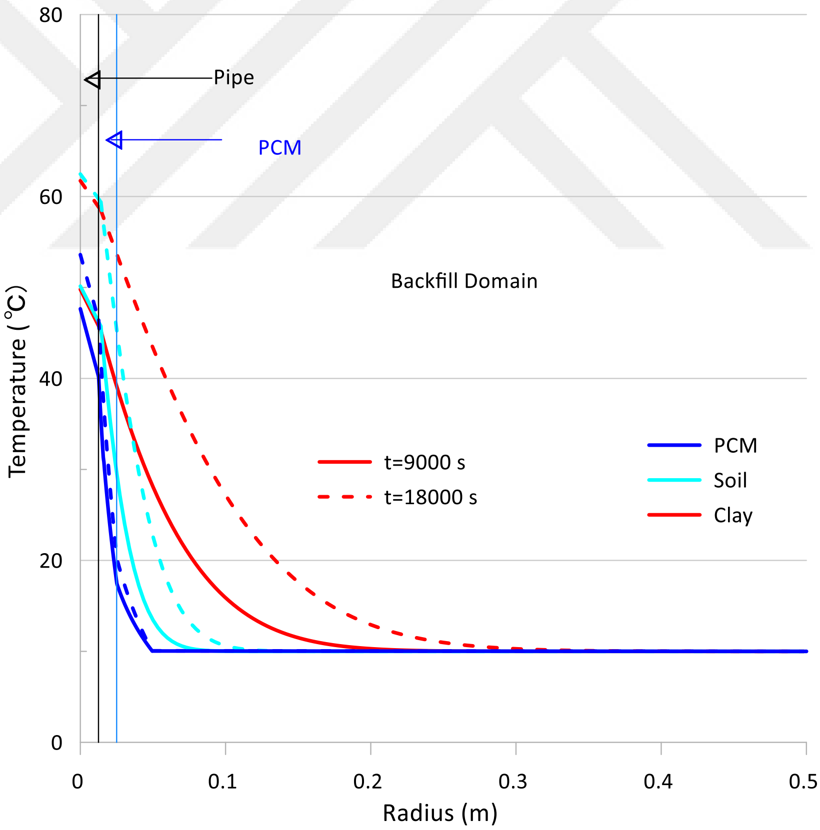

Figure 2.9 Temperature distribution along the radial direction at z=0.250 m

The maximum temperature within the backfill domain is observed adjacent to the pipe. At $t = 9000\ s$, the temperature values for different backfill materials are compared at $r = 0.012606$ m. For clay, soil, and PCM cases the temperature values are observed as 45.27°C, 45.73°C, and 40.17°C, respectively. In advancing time, the temperature increases for all types of backfill materials. At $t = 18000$ s, for the same positions as defined earlier, the temperatures of clay, soil, and PCM are obtained to be 58.48°C, 59.40°C, and 40.41°C, respectively. The spatial temperature changes along the radial direction clearly show that the temperatures are higher when the clay is used as a backfill material. As an instance, at $t = 18000$, the temperatures of clay, soil, and PCM-Soil domain are obtained to be 40.82°C, 19.10°C, and 11.05°C, respectively, for $r = 0.05667$ m. Regarding the heat diffusion performance of the materials, backfill materials can be ordered as clay, soil, and PCM. PCM acts as a thermal insulator and traps the heat near the pipe and prevents heat loss within the backfill domain.

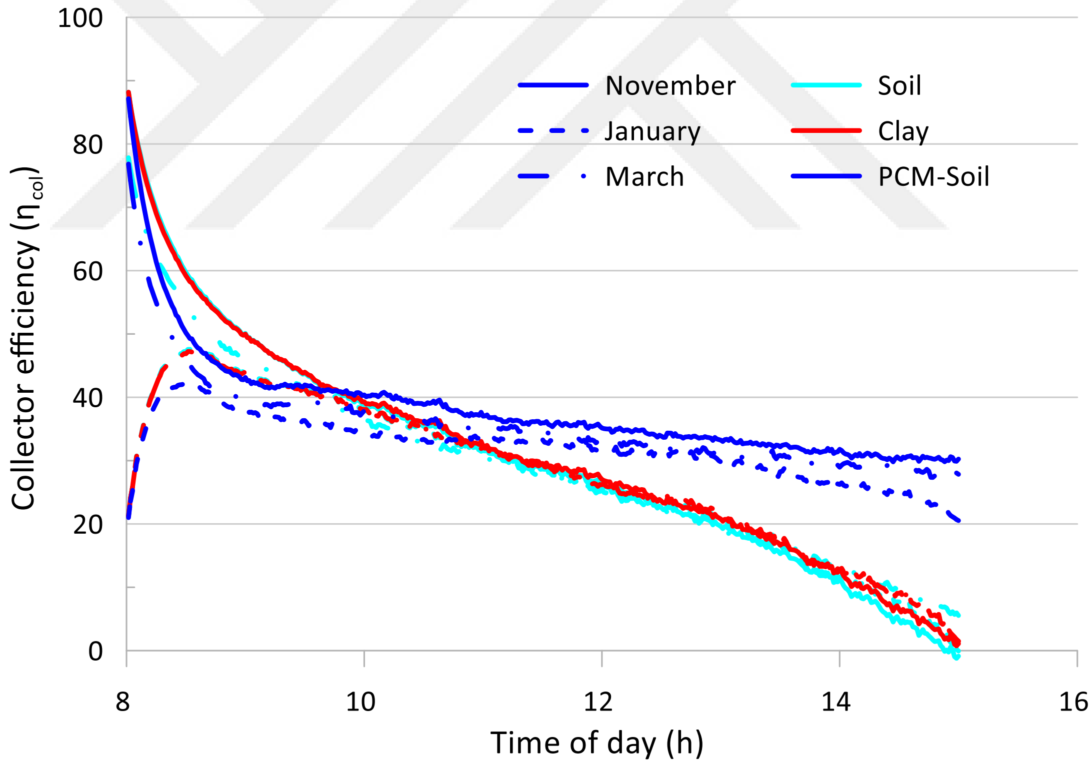

Figure 2.10 Solar collector efficiency in BHE with different backfill materials in heating months

In Figure 2.10, solar collector efficiencies of the solar-assisted BHE unit backfilled with clay, soil, and PCM-soil in November, January, and March are given. Results of solar collector efficiencies of simulations should be assessed by considering the input weather data which is shown in Figure 2.3. The solar collector efficiency (η_{col}) in November is greater than the efficiencies in January and March as the ambient temperature and solar irradiance in November are decent, as expected.

Using clay or soil as backfill materials do not cause any remarkable change in solar collector efficiency. However, integrating PCM into BHE and the usage of a PCM-soil backfill domain has a crucial impact on solar collector efficiency. Although the solar collector efficiency of BHE with PCM-soil domain is lower than the other backfill mediums at the beginning of the charging period, the solar collector efficiency remains stable in advancing time, especially after midday. During this period, the efficiency of the solar collector for BHE with PCM-soil domain is greater than the solar collector efficiency of BHE backfilled with clay or soil. The average solar collector efficiency is 31% for BHE with PCM-soil domain, however, the efficiencies are 27.5 % and 28 % for soil and clay backfilled BHE in January, respectively.

CHAPTER THREE

CYCLIC BEHAVIOR OF A SOLAR ASSISTED TES UNIT WITH PCM

This chapter explains the charging and discharging behaviors of a solar-assisted shell-and-tube thermal energy storage unit with phase change material. At first, a brief explanation of the system composed of solar aided shell and tube TES with PCM integrated with heat pump system is given. Methods that are used in the numerical model is then provided. The chapter is concluded with the parametric results. The effects of the heat demand profile, PCM's latent heat, and the melting temperature are discussed.

3.1 System Description

In this part of the thesis, a numerical model is developed to investigate the cyclic behavior of a heat pump integrated solar-assisted shell-and-tube LHTES unit under real weathear conditions for heating months in Izmir. The solar-assisted shell and tube LHTES unit integrated with a heat pump system consists of a solar collector, pumps, LHTES unit, and heat pump. The schematic view of the system is shown in Figure 3.1.

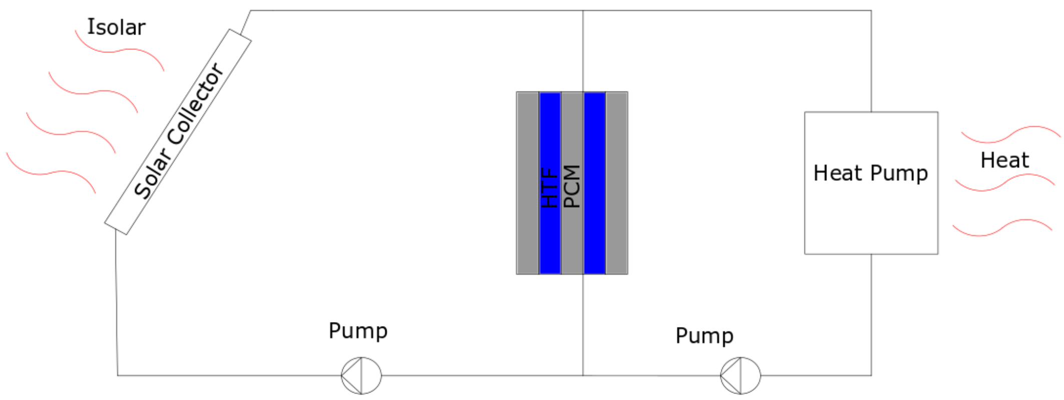

Figure 3.1 Schematic view of the integrated system

In the system, water is used as a HTF and PCM is used as a backfill material within the LHTES. The thermophysical properties of the materials are given in Table 3.1.

Table 3.1 Thermophysical properties of materials

		Thermal conductivity (W/mK)	Specific Heat (J/kg)	Density (m^3/kg)	Sources
Water		0.576	4180	1000	Bergman et al. (2007)
PCM	Solid	0.18	1800	789	Rubitherm (2018)
	Liquid	0.19	2400	750	Rubitherm (2018)

Preliminary parametric runs are undergone to determine the suitable diameter of the shell. The geometrical properties of the solar-assisted shell-and-tube LHTES unit are $D_{pipe} = 0.025\ m$, $D_{PCM} = 0.05\ m$ and $L = 0.5\ m$.

The solar collector's geometrical properties are taken from a recent study developed for Izmir City, Turkey (Alptekin & Ezan, 2020). The solar collector tilt angle is defined by referring to the work of Ülgen (2006), in which the optimum solar collector tilt angle of Izmir City is defined as 30.3°.

3.1.1 Operation conditions

The solar-assisted shell-and-tube LHTES unit integrated with a heat pump system works to supply the heat demand of the house in Izmir. The house's heating demand is defined by referring to Balta, Dinçer & Hepbaşlı (2010). Variations in the house's heating demand and ambient temperature for five different heating months are given in Figure 3.2.

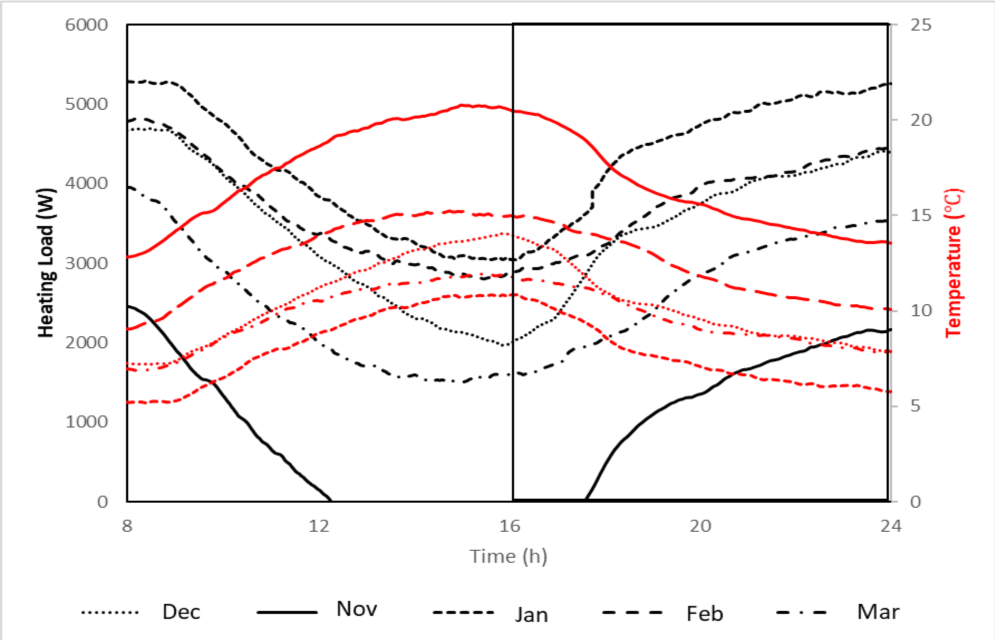

Figure 3.2 Heating demand for house and ambient temperature in heating months

It is essential to determine the operation interval for the charging period of the LHTES unit to decrease the heat loss through the surroundings during the heating months. For this purpose, initial simulations have been conducted to determine the influence of the solar-assisted LHTES unit's starting time on the charging performance. Figure 3.3 shows the variations in the LHTES inlet temperature of the HTF for four different starting times. After these attempts, the most suitable starting time of the charging process is determined as 9 am.

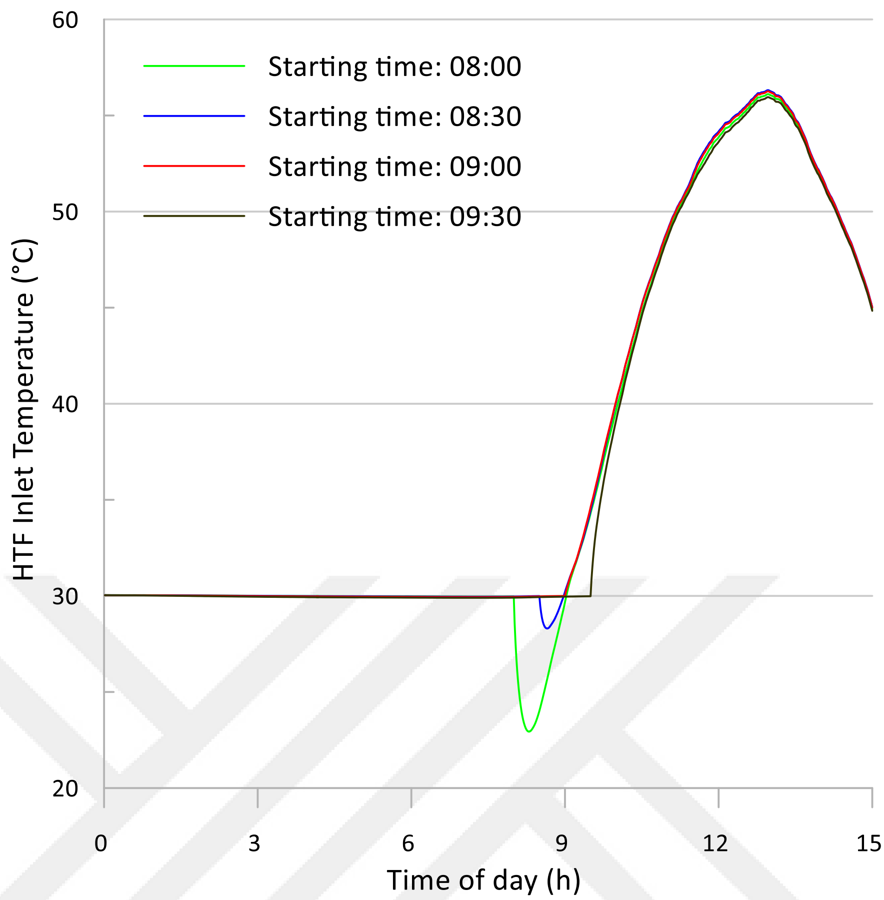

Figure 3.3 Influence of starting time on the evolution of the HTF temperature

The starting time of the discharging process is determined by using the heat demand profile of the house, as shown in Figure 3.2. Except for November, the heat demand increases after 4 pm through midnight. That is, the discharging process starts at 4 pm in December, January, February, and March. However, for November, the discharging process initiates at 6 pm. In preliminary attempts, it is noticed that the HTF temperature decreases after 3 pm. So, the period between 3 pm and 4 pm is selected as the idle period in the model. Consequently, the operating periods of each mode of the system are summarized in Table 3.2.

Table 3.2 Operating periods

Mode of the System	Start Time	End Time
Charging Process	9 am	3 pm
Idle Period	3 pm	4 pm
Discharging Process	4 pm	12 am

3.2 Solution methods

In the numerical model developed to investigate the cyclic behavior of solar-assisted shell-and-tube LHTES unit, the following conditions are considered.

(1) The flow of the HTF is fully developed.
(2) The velocity of the HTF is constant.
(3) The pipes in the system and LHTES tank are well insulated.
(4) The initial temperature of the LHTES domain is uniform and equal to ambient temperature on the simulation time and month.
(5) The natural convection in the PCM domain is neglected.
(6) The radiation effects are neglected.

3.2.1 Governing equations

The energy equation for HTF and PCM can be reduced as follows

for PCM domain:

$$\frac{\partial CT}{\partial t} = \frac{\partial}{\partial z}\left(k\frac{\partial T}{\partial z}\right) + \frac{1}{r}\frac{\partial}{\partial r}\left(kr\frac{\partial T}{\partial r}\right) - \frac{\partial S}{\partial t} \tag{3.1}$$

for working fluid domain:

$$\rho c\frac{\partial T}{\partial t} + \rho cu\frac{\partial T}{\partial z} = \frac{\partial}{\partial z}\left(k\frac{\partial T}{\partial z}\right) + \frac{1}{r}\frac{\partial}{\partial r}\left(kr\frac{\partial T}{\partial r}\right) \tag{3.2}$$

The heat diffusion in the phase change material is modeled by using the fixed grid numerical model of Cao & Faghri (1990).

$$C(T)=\begin{cases}(\rho c)_s & T<T_m-\delta T_m\\ (\rho c)_m+\rho_l\dfrac{h_{sf}}{2\delta T_m} & T_m-\delta T_m\le T\le T_m+\delta T_m\\ (\rho c)_l & T>T_m-\delta T_m\end{cases} \tag{3.3}$$

$$S(T)=\begin{cases}(\rho c)_s(\delta T_m-T_m) & T<T_m-\delta T_m\\ (\rho c)_l(\delta T_m-T_m)+\rho_l\dfrac{h_{sf}}{2\delta T_m}-\rho_l\dfrac{h_{sf}}{2\delta T_m}T_m & T_m-\delta T_m\le T\le T_m+\delta T_m\\ (\rho c)_l(\delta T_m-T_m)-\rho_l h_{sf} & T>T_m-\delta T_m\end{cases} \tag{3.4}$$

The relative temperature difference is used to determine the steady behavior of the cyclic simulation:

$$RTD=\frac{T_{i+1,j}-T_{i,j}}{T_m} \tag{3.5}$$

where $T_{i,j}$ is temperature i is the day, j is the second of the day and $T_{i+1,j}$ is the temperature at next day, T_m is the melting temperature of the PCM.

3.2.2 Heat pump model

Integrating a heat pump system into the solar-assisted LHTES unit is one of the aims of the current thesis. The first law of thermodynamics is used to integrate the heat pump into the system (Çengel & Boles, 2007).

$$\sum\dot{E}_{in}=\sum\dot{E}_{out} \tag{3.6}$$

The energy balance of the control volume can be reduced as follows

$$\dot{W}_{comp}+\dot{Q}_{evap}=\dot{Q}_{cond} \tag{3.7}$$

where $\dot{W}_{comp}$ represents compressor work, $\dot{Q}_{evap}$ represents the inlet heat energy of the evaporator, and $\dot{Q}_{cond}$ is the heat energy of the condenser. The heat demand of the house in the simulation day is given as $\dot{Q}_{cond}$ in the heat pump system.

$$COP = \frac{\dot{Q}_{cond}}{\dot{W}_{comp}} \tag{3.8}$$

The coefficient of performance (COP) is used to assess the performance of the heat pump. A COP correlation for solar energy assisted water sourced and air source heat pump systems are represented in Kaygusuz (1995) study. These correlations can be used to determine the COP of the heat pump system. The correlation is written following.

for a heat pump with water source system:

$$COP_{water} = 5.46 + 5.33 \times 10^{-2} T_w - 5.33 \times 10^{-4} T_w^2 + 1.20 \times 10^{-6} T_w^3 \tag{3.9}$$

for the heat pump with air source system:

$$COP_{air} = -27.86 + 0.121 T_a + 1.601 \times 10^{-4} T_a^2 - 7.035 \times 10^{-7} T_a^3 \tag{3.10}$$

3.2.3 Solution procedure

In the numerical method, variable weather data of Izmir City is defined into the code, and the solar collector sub-function solves the related equations, i.e., Equations. 2.11 and 2.12, to calculate the outlet temperature of the HTF from the flat plate solar collector. The outlet temperature of HTF for the solar collector is then specified as the inlet temperature of the LHTES unit. The control volume method is applied for the HTF and the backfill domains to transform the governing equations for each domain, i.e., Equations. 3.1 and 3.2, into algebraic form. The final set of algebraic equations is then iteratively solved with SIS (Strongly Implicit Solver) algorithm with 10^{-8} tolerance. The convergence criteria in the model assumed as 10^{-7} after several attempts. Also, grid size and time step concluded after many preliminary analyses as 100×60 and 1 s respectively. The COP of the integrated heat pump is calculated with the HTF outlet temperature with the Equations. 3.6 to 3.10 are iteratively solved in MATLAB to determine the response of the integrated system, which involves the flat plate collector and the LHTES and heat pump system.

3.3 Results & Discussion

In this section, the effects of heat demand profile, latent heat of the PCM, and melting temperature of the PCM are investigated and results of the simulations for consecutive seven days in heating months are given in the following subsections.

3.3.1 Cyclic behavior of the solar-assisted LHTES unit

It is essential to carry out simulations for certain repetitive days to eliminate initial temperature fields' influence on the evaluated results. Herein, the simulations are run for seven consecutive days to ensure that the influence of initial temperature is diminished. In Figure 3.4, mean PCM temperature and the relative temperature difference between selected days in December for PCM which has different latent heat values Figure 3.4(a) is for $L_h = 165$ kJ/kg and Figure 3.4(b) is for $L_h = 240$ kJ/kg. The relative temperature difference (RTD) is determined by using Equation 3.5. The mean PCM temperature is lowest on the 3^{rd} working day. The RTD decreases as the simulation proceeds and the temperature variations on the 5^{th} day and 7^{th} day are fairly close. For PCM with a higher latent heat value, the variations at the initial days look more significant. In each case, the RTD has a similar pattern for two PCMs; the RTD value for the 5th and 7th days is lower than 0.01 C.

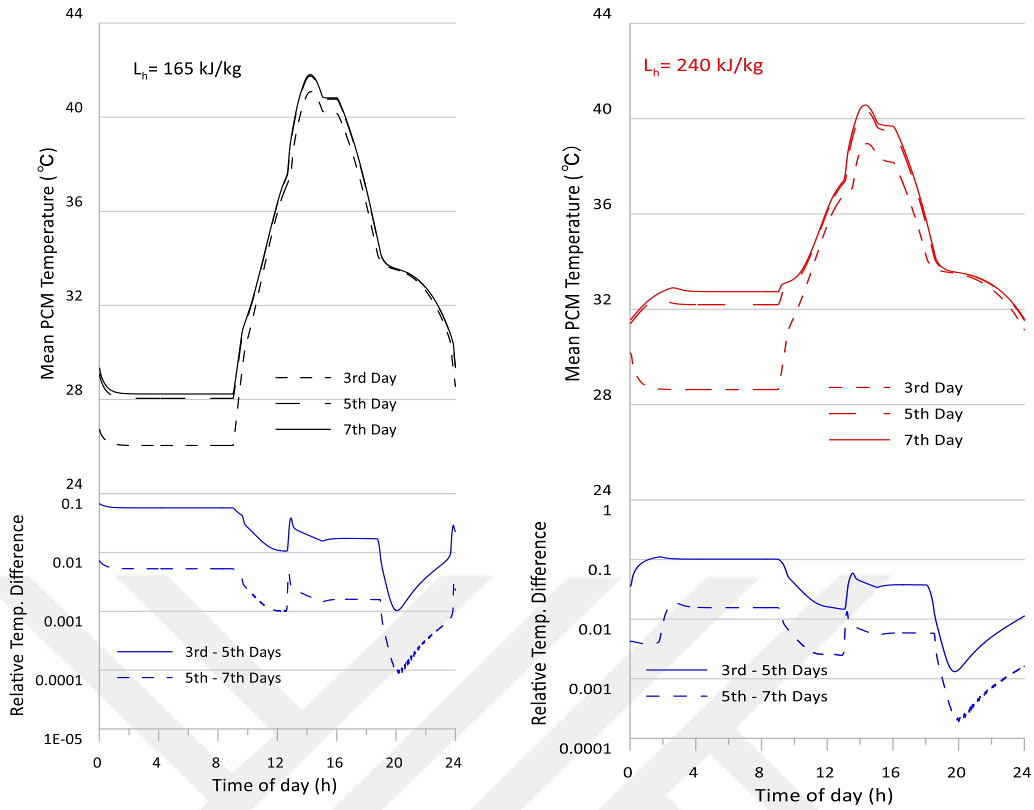

(a) $L_h = 165\ kJ/kg$ (b) $L_h = 240\ kJ/kg$

Figure 3.4 Mean PCM temperature and relative temperature difference

3.3.2 Effects of the heat demand profile

The influence of the constant heat demand on the solar-assisted shell-and-tube LHTES unit can be seen in Figure 3.5. The constant heat demand causes instant high discharge from the LHTES unit. Such a high heat transfer rate causes a rapid temperature drop and quick solidification in the PCMs. Real weather data of heating months and the heating demand value determine the time for complete solidification. In February, PCMs are fully solidified at 11.30 pm; however, PCMs are fully solidified at 9 pm in December and January. The mean PCM temperature and liquid fraction of the PCM, which has a melting temperature of 35°C on the discharging period for three different heating months, are given in Figure 3.5. The results of the 5th simulation day in December is shown in Figure 3.5(a). The mean PCM temperature starts to decrease with the discharging process from 41°C and 39°C for PCMs with $L_h = 165$ kJ/kg and $L_h = 240$ kJ/kg, respectively. The PCM is in the liquid phase at the beginning of the discharging process. At the end of the discharging process, mean PCM temperatures are $28.$ ℃ and 31.9℃ for PCMs with $L_h = 165$ kJ/kg and $L_h = 240$ kJ/kg, respectively. PCMs, turn into a solid phase at the end of the discharging period in each case.

In Figure 3.5 (b), the simulation results of the 5th simulation day in January are given. At the start of the discharging process, the mean temperature of PCMs are 43.8 ℃ and 42 ℃ for PCMs with $L_h = 165\ kJ/kg$ and $L_h = 240\ kJ/kg$ respectively. PCMs are fully melted at the beginning and start to melt with discharging time. After $21{:}30$ PCMs are fully solidified for every case. At the end of the discharging process, mean PCM temperatures are 24.9 ℃ and 30.6 ℃ for PCMs with $L_h = 165\ kJ/kg$ and $L_h = 240\ kJ/kg$ respectively.

The simulation results of the 5th simulation day in February are given in Figure 3.5(c). Mean temperature of PCMs are 47℃ and 46℃ at the beginning and decreases with discharging time by 32℃ and 33℃ at the end of the discharging period for PCMs with $L_h = 165$ kJ/kg and $L_h = 240$ kJ/kg, respectively. PCMs begin to solidify at the start of the period, and PCMs are fully solidified at 11 pm.

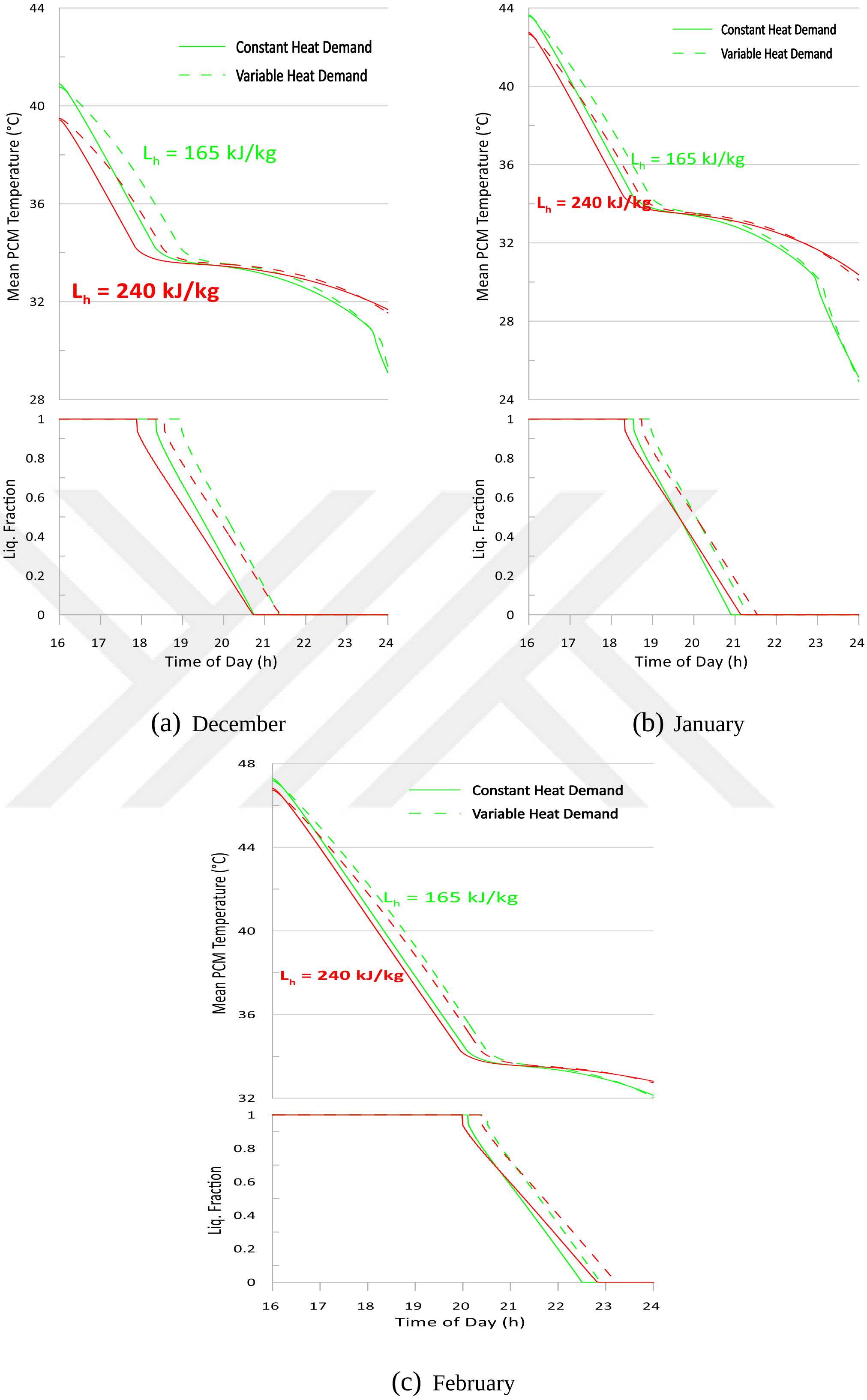

Figure 3.5 Mean PCM temperature and liquid fraction of PCM with different heat demand in (a) December (b) January (c) February

The PCMs melts in the early days of the simulations and do not solidify in November and March due to the low heat requirement. The LHTES unit is being out of its purpose and behaves like a sensible heat storage tank.

3.3.3 Effects of latent heat of PCM

Effects of variation in latent heat of PCM on the LHTES unit with variable heating demand can be seen in Figure 3.6. Here PCM with a melting temperature of 35℃ is used. Although, the mean temperature of PCM with $L_h = 240$ kJ/kg is greater at the beginning of the charging process; at the end of the charging period, its temperature is lower than the PCM with $L_h = 165$ kJ/kg. Variation in latent heat of PCM has little impact on liquid fraction, the duration that PCM is fully melted decreases with an increase in latent heat of PCM.

In Figure 3.6 (a), the results of the 5th simulation day in December are given. Mean temperature of the PCM with $L_h = 165$ kJ/kg is 28℃ at the beginning of the charging, the temperature increases with time until the midday of the simulation. At the beginning of the idle period, PCM with $L_h = 165$ kJ/kg has a greater temperature. Although the temperature of the PCM with $L_h = 240$ kJ/kg has less temperature within the idle period, at the end of the discharging process the temperature is greater than the PCM which has $L_h = 240$ kJ/kg with 31.8℃.

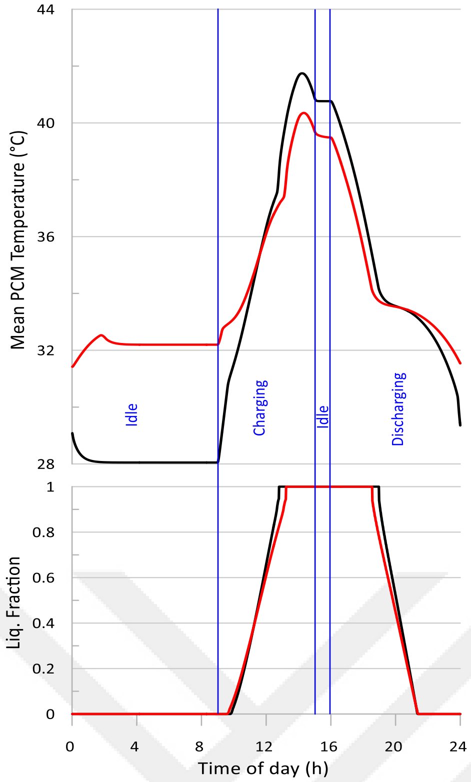

(a) December

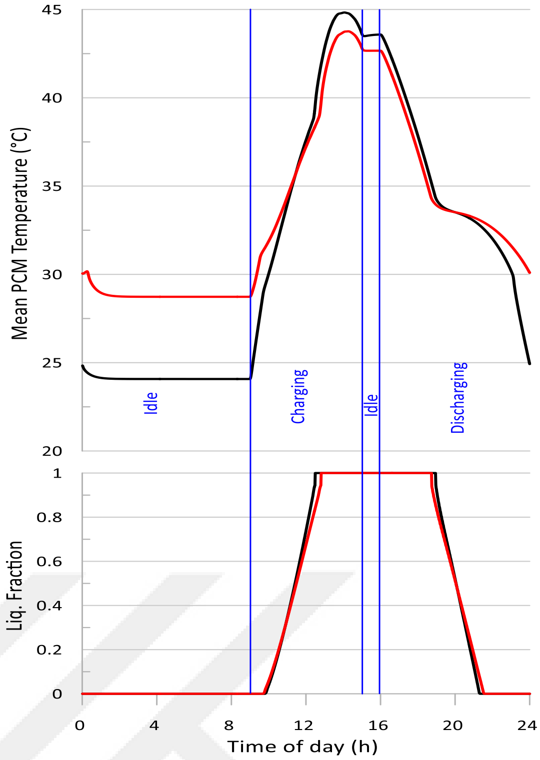

(b) January

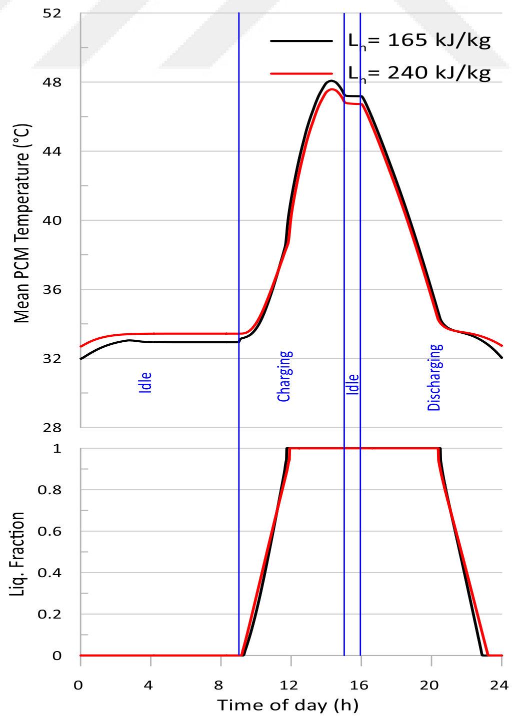

(c) February

Figure 3.6 Mean PCM temperature and liquid fraction of PCM with the different latent heat of PCM in (a) December (b) January (c) February

The 5th simulation day results of the simulations in January are given in Figure 3.6 (b). Mean temperature of the PCM with $L_h = 240$ kJ/kg is 29℃, the temperature of PCM with $L_h = 165$ kJ/kg is 26℃ at the beginning of the charging, the temperature increases with time until midday of the simulation. At the beginning of the idle period, PCM with $L_h = 165$ kJ/kg has a greater temperature. Although the temperature of the PCM with $L_h = 240$ kJ/kg has less temperature within the idle period, at the end of the discharging process, the temperature is greater than the PCM which has $L_h = 240$ kJ/kg with 30℃. The mean temperature of the PCM with $L_h = 165$ kJ/kg is 25℃. All PCMs melts with the charging period and solidify with the discharging period.

In Figure 3.6 (c), the results of the 5th simulation day in February are given. Mean temperature of the PCM with $L_h = 165$ kJ/kg is 32℃ at the beginning of the charging, the temperature increases with time until the midday of the simulation. At the beginning of the idle period, PCM with $L_h = 165$ kJ/kg has a greater temperature. Although the temperature of the PCM with $L_h = 240$ kJ/kg has less temperature within the idle period, at the end of the discharging process the temperature is greater than the PCM which has $L_h = 240$ kJ/kg with 33℃.

In November and March, increasing in latent heat of PCM does not have a crucial impact on the cyclic behavior of the solar-assisted LHTES unit. The PCM domain melts in earlier simulation days and never solidifies due to low heat demand in November and March. The LHTES unit is being used out of objective and behaves like a sensible storage tank after 2 simulation days.

3.3.4 Effects of melting temperature of PCM

Influence of melting temperature of PCM which has $L_h = 240$ kJ/kg on LHTES unit with variable heat demand profile is given in Figure 3.7. The increasing melting temperature of PCM affects the melting and solidification process directly. So, the PCM with greater melting temperature melts later, solidifies earlier than others. The mean temperature of all PCMs increases with the charging period concerning time. When $T_m = 31$℃, temperature at the end of the charging period is greater than other types of PCMs. However, the mean temperature of PCM with $T_m = 31$℃ decreases with discharge. The PCM with $T_m = 40$℃ mean temperature less than other types of PCMs at the end of the charging period.

In Figure 3.7 (a), the results of the 5th simulation day in December are given. The mean temperature of PCM with $T_m = 31$℃ goes up to 42℃, the temperature of the PCM which has $T_m = 35$℃ increases up to 40℃ and PCM temperature with $T_m =$ 40℃ goes up to 39℃ at maximum on the 5th day of simulation. PCMs temperature with $T_m = 31$℃, $T_m = 35$℃ and $T_m = 40$℃ are 29℃, 32℃, and 28℃ at the end of the discharging period, respectively. The PCM with $T_m = 40$℃ does not melt during the charging period and easily solidifies with discharge.

The 5th simulation day results in January are given in Figure 3.7 (b). The mean temperature of PCMs with $T_m = 31$℃, $T_m = 35$℃ and $T_m = 40$℃ are 43.8℃, 42.4℃ and 41℃ in the second idle period, respectively. At the end of the discharging period, the mean temperature of PCM with $T_m = 40$℃ is 27.5℃ and less than other types of PCMs. Also, the PCM with $T_m = 40$℃ melts earlier than others.

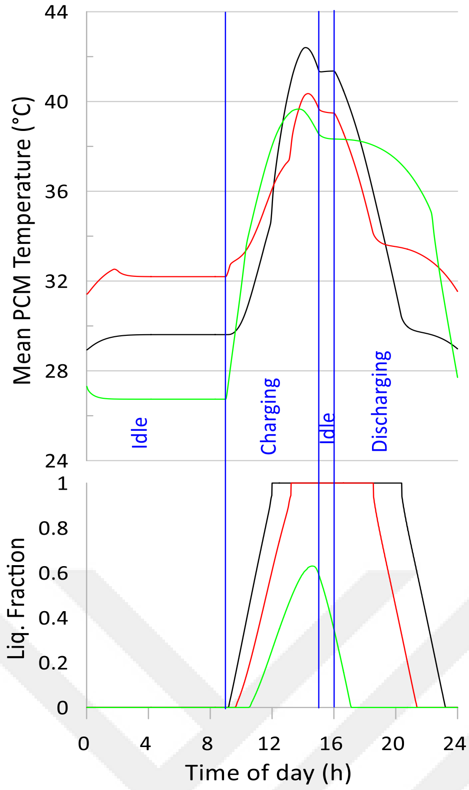

(a) December

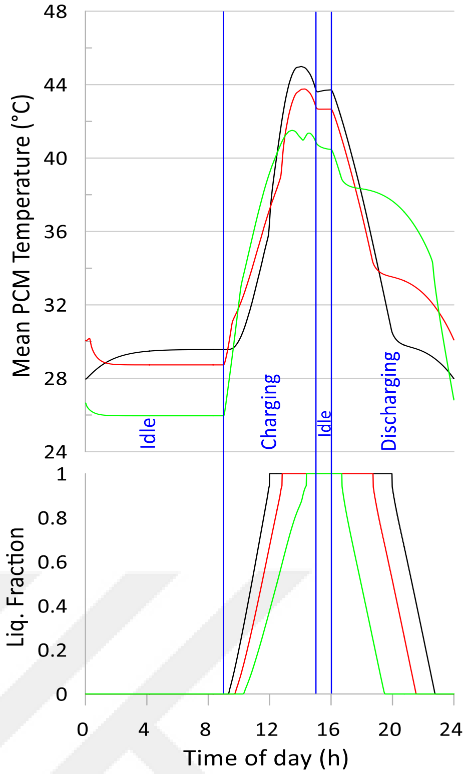

(b) January

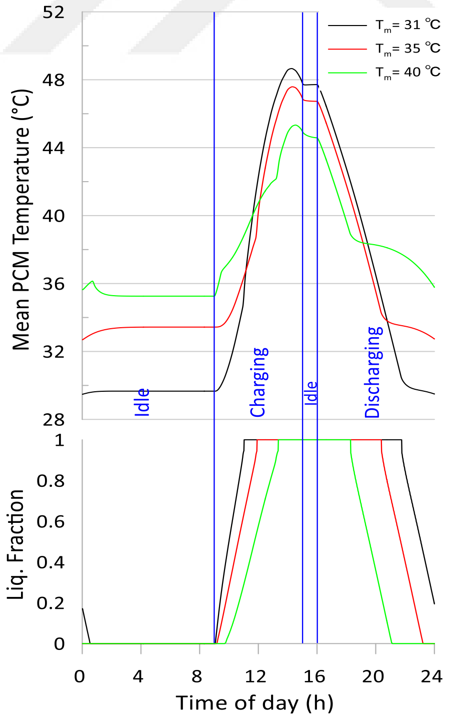

(c) February

Figure 3.7 Mean PCM temperature and liquid fraction of PCM with a different melting temperature of PCM in (a) December (b) January (c) February

In Figure 3.7 (c), the results of the 5th simulation day in February are given. Mean temperature of the PCM with $T_m = 35$℃ is 33.5℃ at the beginning of the charging, the temperature increases with time until midday of the simulation. At the beginning of the idle period, PCM with $T_m = 31$℃ has a greater temperature. Although the temperature of the PCM with $T_m = 40$℃ has less temperature within the idle period, at the end of the discharging process the temperature is greater than other PCMs.

It can be seen in Figure 3.7, weather conditions also have an impact on the simulation results of the mean temperature of PCM. The solar irradiation in February heats the HTF and the HTF melts PCM with $T_m = 40$℃. At the end of the discharging period temperature of PCM ($T_m = 40$℃) is 36℃ and is greater than simulations in other heating months and all types of PCMs.

Increasing melting temperature of PCM has an essential effect on the melting and solidification process in heating months. However, this effect cannot be seen in November and March. When $T_m = 40$℃ the PCM still melts early of cyclic simulation. The HTF inlet temperature increases up to approximately 60℃ in November and March. Solar irradiance and ambient temperature data cause this effect and are being a reason for misuse of the LHTES unit.

3.3.5 Energetic evaluation of the systems

Several studies have been conducted on the evaluation of the integration of solar energy into heating and cooling systems. As a result of these studies, it has been focused on either the supplying evaporator energy needs of the heat pump with solar collectors or the compressor requirement with PV systems. Considering the existence of very important environmental problems today, heat pump systems supported by renewable energy sources gain importance.

The influence of the integrating solar-assisted LHTES unit with $L_h = 240$ kJ/kg, $T_m = 35$℃ into the heat pump system with variable heat demand in December, January, and February is shown in Figure 3.8. It is seen that the LHTES integrated heat pump system operating between 4 pm – 12 am is compared with the COP and compressor work requirement of the air source heat pump that operates at the same time interval. As can be seen, when the LHTES unit is integrated, the system that reaches the highest COP value when the operation starts decreases with the discharge. However, the COP value is quite high during the working periods in comparison with w/out LHTES value.

Considering the compressor needs, it increases in both cases after the heat pump system starts to work. In the case of w/out the LHTES unit, this increase depends on the air temperature, in the case of the LHTES unit, it depends on the temperature falling in the tank due to discharge. However, there is a difference of close to 385 W between the two cases.

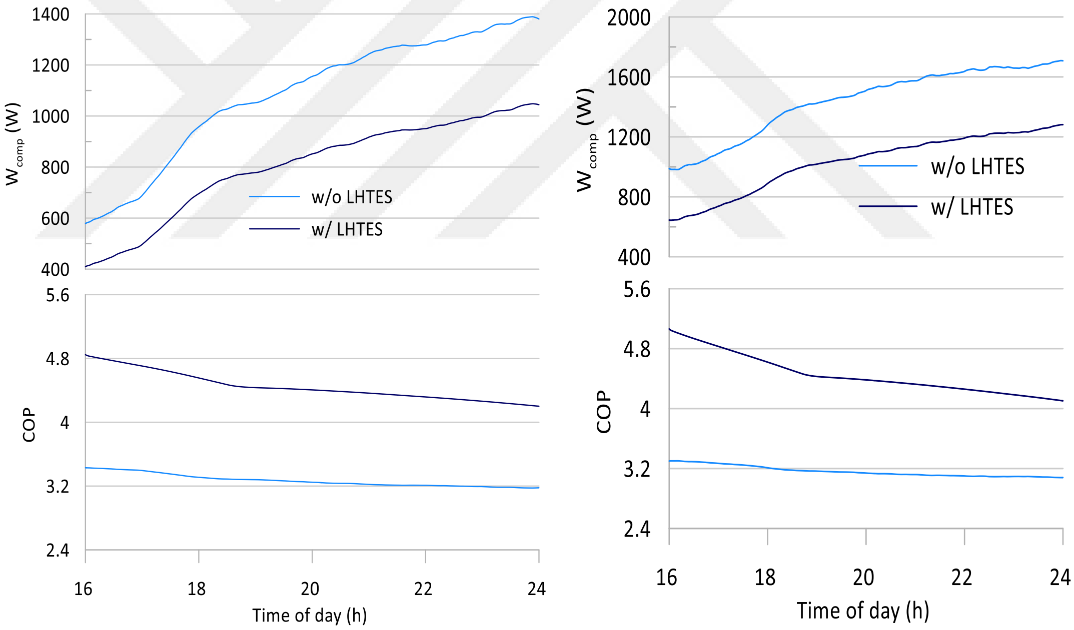

(a) December (b) January

Figure 3.8 Compressor work and COP of heat pump integrated with LHTES in (a) December, (b) January and (c) February

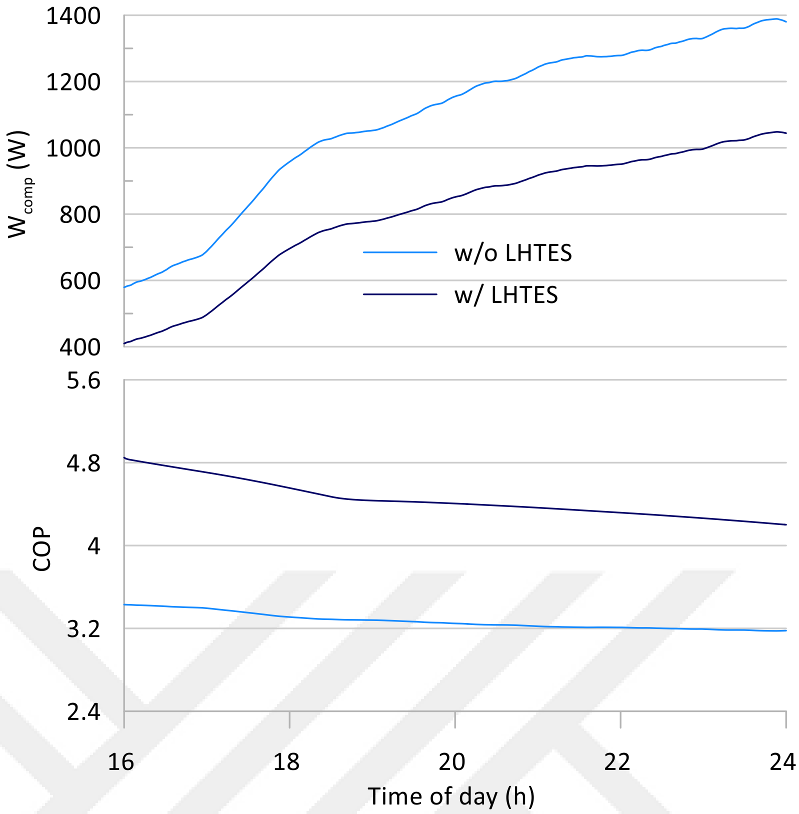

(c) February

Figure 3.8 continues

The real weather data in heating months has also an effect on the solar-assisted LHTES integrated with a heat pump system. In Figure 3.9, compressor work and COP are given in simulation heating months for the LHTES filled with PCM that has $L_h = 240$ kJ/kg and $T_m = 35$°C.

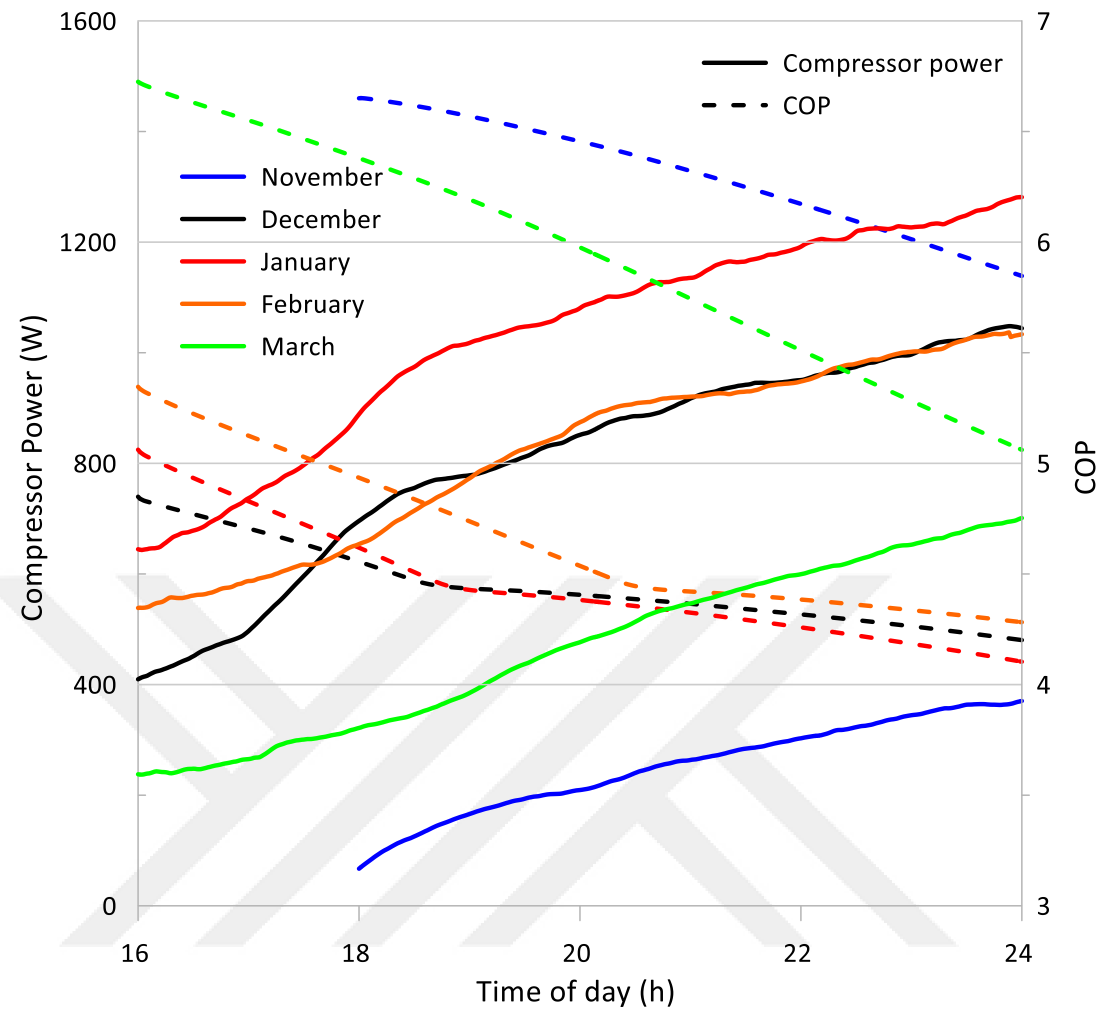

Figure 3.9 Compressor work and COP of the heat pump in heating months

In November, the heat pump system starts the operation, and the discharging period begins at 6 pm, in other heating months starts at 4 pm. The COP of the heat pump decreases, and compressor work decreases with time in all heating months. As illustrated in Figure 3.9, weather conditions are the key factor for the solar-assisted LHTES unit integrated with the heat pump, since weather conditions have an important impact on performance issues of the heat pump.

Also, the effects of a solar-assisted LHTES unit integrated with a heat pump on COP of the heat pump system is shown in Table 3.4 in comparison with the average COP of an air source heat pump in the same heating months.

Table 3.3 Increment in COP

Type of PCM		**Months**	**COP w/ LHTES**	**COP w/o LHTES**	**COP increment**
T_m (°C)	**L_h (kJ/kg)**				
31	**165**	November	6.22	3.46	80%
		December	4.36	3.26	34%
		January	4.32	3.16	37%
		February	4.56	3.24	41%
		March	5.78	3.35	73%
	240	November	6.22	3.46	80%
		December	4.35	3.26	33%
		January	4.33	3.16	37%
		February	4.56	3.24	41%
		March	5.78	3.35	73%
35	**165**	November	6.22	3.46	80%
		December	4.4	3.26	35%
		January	4.39	3.16	39%
		February	4.59	3.24	42%
		March	5.78	3.35	73%
	240	November	6.22	3.46	80%
		December	4.4	3.26	35%
		January	4.4	3.16	39%
		February	4.59	3.24	42%
		March	5.78	3.35	73%
40	**165**	November	6.22	3.46	80%
		December	4.47	3.26	37%
		January	4.48	3.16	42%
		February	4.67	3.24	44%
		March	5.78	3.35	73%
	240	November	6.22	3.46	80%
		December	4.49	3.26	38%
		January	4.49	3.16	42%
		February	4.67	3.24	44%
		March	5.78	3.35	73%

CHAPTER FOUR

CONCLUSION

In the first stage of the current thesis, a solar assisted borehole heat exchanger unit with a different backfill domain is simulated with the numerical model developed in a MATLAB environment under real weather conditions for heating months. Effects of different backfill materials and integrating PCM into the BHEs backfill domain on charging process of the BTES, on thermal influence radius, on solar collector efficiency, and real weather conditions are investigated, and results are discussed. The following concluding remarks can be listed as:

- Weather conditions have an essential impact on the charging behavior of solar-assisted BTES units. As an example, the inlet temperature of heat transfer fluid goes up to 64 ℃, and the mean temperature of clay is 13.5℃ in March. However, the temperature of HTF is 45℃ and the mean temperature of clay is 12 ℃ in January.
- The effect of different backfill material on thermal influence radius depends on the thermophysical properties of the material. Clay backfilled BHE unit within BTES causes heat diffusion within the domain by its thermal conductivity value and integrating PCM into BHE within BTES prevents the heat diffusion in the domain and stores energy around the pipe.
- Solar collector efficiency is affected by solar irradiance and ambient temperature. In BTES integrated with solar collector, the backfill material of BHE in BTES can affect the performance of the solar collector. When the PCM is implemented with BHE, solar collector efficiency is greater than other backfill domains
- Integrating PCM into BHE has essential impacts on the charging behavior of solar aided BTES unit as increasing solar collector efficiency and preventing heat diffusion in the backfill domain.

In the second stage of the thesis, the cyclic behavior of the solar-assisted LHTES unit integrated with heat pump is simulated to examine the effects of changes in thermophysical properties of the PCM and influence of heat demand profile of heat pump under real weather conditions. Also, the effects of the implementation of a solar-assisted LHTES unit into the heat pump are discussed in an energetic view. Conclusions can be listed as:

- Weather conditions have an essential impact on the solar aided LHTES integrated with heat pump rather than heat demand profile.
- Increasing the latent heat of PCM does not make many differences in cyclic behavior of the solar aided LHTES unit integrated with heat pump, however, increasing latent heat occurs an increase in stored energy.
- Increasing melting temperature affects the cyclic behavior of the LHTES unit and causes a rapid temperature to decrease in the PCM temperature in the discharging period in December and January.
- Integration of solar-assisted LHTES unit into heat pump decreases the compressor work and increases COP.

REFERENCES

Alptekin, E., & Ezan, M. A. (2020). Performance investigations on a sensible heat thermal energy storage tank with a solar collector under variable climatic conditions. *Applied Thermal Engineering*, *164*, 114423.

Balta, M. T., Dincer, I., & Hepbasli, A. (2010). Performance and sustainability assessment of energy options for building HVAC applications. *Energy and Buildings*, *42*(8), 1320-1328.

Başal, B., & Ünal, A. (2013). Numerical evaluation of a triple concentric-tube latent heat thermal energy storage. *Solar Energy*, *92*, 196-205.

Bauer, D., Heidemann, W., & Diersch, H. J. (2011). Transient 3D analysis of borehole heat exchanger modeling. *Geothermics*, *40*(4), 250-260.

Bergman, T. L., Incropera, F. P., DeWitt, D. P., & Lavine, A. S. (2011). *Fundamentals of heat and mass transfer* (7th ed.). New Jersey: John Wiley & Sons.

Biglarian, H., Abbaspour, M., & Saidi, M. H. (2017). A numerical model for transient simulation of borehole heat exchangers. *Renewable Energy*, *104*, 224-237.

Bottarelli, M., Bortoloni, M., Su, Y., Yousif, C., Aydın, A. A., & Georgiev, A. (2015). Numerical analysis of a novel ground heat exchanger coupled with phase change materials. *Applied Thermal Engineering*, *88*, 369-375.

Cao, Y., & Faghri, A. (1990). A numerical analysis of phase-change problems including natural convection. *Journal of Heat Transfer*, *112*(3),812-816.

Cao, Y., & Faghri, A. (1991). Performance characteristics of a thermal energy storage module: a transient PCM/forced convection conjugate analysis. *International Journal of Heat and Mass Transfer*, *34*(1), 93-101.

Cui, P., Yang, H., & Fang, Z. (2008). Numerical analysis and experimental validation of heat transfer in ground heat exchangers in alternative operation modes. *Energy and Buildings*, *40*(6), 1060-1066.

Cengel, Y. A., & Boles, M. A. (2007). *Thermodynamics: An Engineering Approach 6th Editon (SI Units)*. New York: The McGraw-Hill Companies.

Dincer, I., & Ezan, M. A. (2018). *Heat Storage: A Unique Solution for Energy Systems*. Switzerland: Springer.

Duffie, J. A., & Beckman, W. A. (2013). *Solar engineering of thermal processes* (4^{th} ed.) New Jersey: John Wiley & Sons

Elbahjaoui, R., El Qarnia, H., & Naimi, A. (2018). Thermal performance analysis of combined solar collector with triple concentric-tube latent heat storage systems. *Energy and Buildings*, *168*, 438-456.

Eskilson, P., & Claesson, J. (1988). Simulation model for thermally interacting heat extraction boreholes. *Numerical Heat Transfer*, *13*(2), 149-165.

Gong, Z. X., & Mujumdar, A. S. (1997). Finite-element analysis of cyclic heat transfer in a shell-and-tube latent heat energy storage exchanger. *Applied Thermal Engineering*, *17*(6), 583-591.

Hellström, G. (1991). *Ground Heat Storage: Thermal Analyses of Duct Storage Systems.-1: Theory*, Ph.D. Thesis, Lund Institute of Technology, Lund University, Lund. SW.

Hollands, K. G. T., Unny, T. E., Raithby, G. D., & Konicek, L. (1976). Free convective heat transfer across inclined air layers. *Journal of Heat Transfer 98(2),*189-193

Huang, H., Xiao, Y., Lin, J., Zhou, T., Liu, Y., & Zhao, Q. (2020). Improvement of the efficiency of solar thermal energy storage systems by cascading a PCM unit with a water tank. *Journal of Cleaner Production*, *245*, 118864.

International Energy Agency. (2020). *Key world energy statistics*. Paris: International Energy Agency.

Kant, K., Shukla, A., Sharma, A., & Biwole, P. H. (2018). Melting and solidification behaviour of phase change materials with cyclic heating and cooling. *Journal of Energy Storage*, *15*, 274-282.

Kaygusuz, K. (1995). Performance of solar-assisted heat-pump systems. *Applied Energy*, *51*(2), 93-109.

Lee, S. L. (1990). A strongly implicit solver for two-dimensional elliptic differential equations. *Numerical Heat Transfer, Part B Fundamentals*, *16*(2), 161-178.

Li, X., Tong, C., Duanmu, L., & Liu, L. (2016). Research on U-tube heat exchanger with shape-stabilized phase change backfill material. *Procedia Engineering*, *146*, 640-647.

Mehta, D. S., Solanki, K., Rathod, M. K., & Banerjee, J. (2019). Influence of orientation on thermal performance of shell and tube latent heat storage unit. *Applied Thermal Engineering*, *157*, 113719.

Rees, S. J., & He, M. (2013). A three-dimensional numerical model of borehole heat exchanger heat transfer and fluid flow. *Geothermics*, *46*, 1-13.

Rubitherm Technologies GmbH (n.d.). Retrieved March 7, 2020, from https://www.rubitherm.eu/en/index.php/productcategory/organische-pcm-rt

Seddegh, S., Wang, X., & Henderson, A. D. (2015). Numerical investigation of heat transfer mechanism in a vertical shell and tube latent heat energy storage system. *Applied Thermal Engineering*, *87*, 698-706.

Seddegh, S., Wang, X., & Henderson, A. D. (2016). A comparative study of thermal behaviour of a horizontal and vertical shell-and-tube energy storage using phase change materials. *Applied Thermal Engineering*, *93*, 348-358.

Tao, Y. B., & He, Y. L. (2011). Numerical study on thermal energy storage performance of phase change material under non-steady-state inlet boundary. *Applied Energy*, *88*(11), 4172-4179.

Trp, A. (2005). An experimental and numerical investigation of heat transfer during technical grade paraffin melting and solidification in a shell-and-tube latent thermal energy storage unit. *Solar Energy*, *79*(6), 648-660.

Trp, A., Lenic, K., & Frankovic, B. (2006). Analysis of the influence of operating conditions and geometric parameters on heat transfer in water-paraffin shell-and-tube latent thermal energy storage unit. *Applied Thermal Engineering*, *26*(16), 1830-1839.

Ulgen, K. (2006). Optimum tilt angle for solar collectors. *Energy Sources, Part A: Recovery, Utilization, and Environmental Effects*, *28*(13), 1171-1180.

Wang, W. W., Zhang, K., Wang, L. B., & He, Y. L. (2013). Numerical study of the heat charging and discharging characteristics of a shell-and-tube phase change heat storage unit. *Applied Thermal Engineering*, *58*(1-2), 542-553.

Yu, X., Li, Z., Lu, Y., Huang, R., & Roskilly, A. P. (2019). Investigation of organic Rankine cycle integrated with double latent thermal energy storage for engine waste heat recovery. *Energy*, *170*, 1098-1112.

APPENDICES

LIST of SYMBOLS

A	area (m^2)
c	specific heat (J/kg K)
D	diameter (m)
$\dot{E}$	rate of energy (W)
H	height (m)
h	convective heat transfer coefficient (W/m^2K)
I_{solar}	incident solar radiation (W/m^2)
k	thermal conductivity (W/mK)
Nu	Nusselt number (–)
R	thermal resistance (℃/m)
$\dot{Q}_u$	useful heat (W)
r	radial coordinate (m)
T	temperature (°C or K)
t	time (s)
u	velocity (m/s)
W	width (m)
z	cartesian coordinate (m)

Greek letters

α	absorptivity of glass (–)
ρ	density (kg/m^3)
σ	Stefan-Boltzmann constant ($W/m^2\ K^4$)

τ	transmissivity of glass (–)
β	collector tilt angle (°)
η	efficiency (−)

Subscripts

amb	ambient
col	collector
comp	compressor
conv	convective
in	inlet
out	outlet

Superscripts

BHE	borehole heat exchanger
BTES	borehole thermal energy storage
COP	coefficient of performance
LHTES	latent heat thermal energy storage
TES	thermal energy storage